Published April 5, 2010

JEM

differentiation, such as those identified here, have been sought. Thus, our study provides new insight into regulation of osteoclastogenesis and bone homeostasis and forms the basis for developing novel therapeutic approaches to treat skeletal disorders.

MATERIALS AND METHODS

Mice. *Bcl6*$^{-/-}$ mice on a mixed C57BL/6 X 129/Sv background were generated by crossing *Bcl6* heterozygotes (*Bcl6*$^{+/-}$; Fukuda et al., 1997). Osteoclast-specific Blimp1 cKO mice on a C57BL/6 background were generated from three lines: mice carrying *loxP*-flanked *Blimp1* alleles (*Blimp1*$^{flox/flox}$; Ohinata et al., 2005), mice harboring *Cre* in the *Ctsk* (*Ctsk*$^{Cre/-}$) locus (Nakamura et al., 2007), and *Blimp1* heterozygotes (*Blimp1*$^{+/-}$; provided by A. Tarakhovsky, The Rockefeller University, New York, NY). Animals were maintained under specific pathogen–free conditions in animal facilities certified by the Keio University School of Medicine animal care committee. Animal protocols were approved by the Keio University School of Medicine animal care committee.

In vitro osteoclast formation. BM cells isolated from long bones (femurs, tibias, and humerus) were cultured 72 h in αMEM (Sigma-Aldrich) containing 10% heat-inactivated FBS (JRH Biosciences) and GlutaMax supplemented with M-CSF (50 ng/ml; Kyowa Hakko Kirin Co.). Adherent cells were then collected for analysis. 10^5 cells were cultured with M-CSF and recombinant soluble RANKL (25 ng/ml; PeproTech Ltd.) for indicated time periods. Mouse spleen cells were cultured overnight in αMEM containing 10% heat-inactivated FBS and GlutaMax supplemented with M-CSF. After this incubation, nonadherent cells were collected and 10^5 cells were cultured with M-CSF and recombinant soluble RANKL (5 or 25 ng/ml) for the indicated time periods. Osteoclastogenesis was evaluated by TRAP and May-Grünwald Giemsa staining (Miyamoto et al., 2000; Yagi et al., 2005). RAW264.7 cells were maintained in αMEM containing 10% heat-inactivated FBS and GlutaMax and stimulated by recombinant soluble RANKL to induce osteoclast formation.

Pit formation assay. Bone resorbing activity of osteoclasts was analyzed as previously described (Iwamoto et al., 2004). In brief, osteoclast precursors isolated from indicated mice were seeded on dentin slices and cultured in the presence of M-CSF plus RANKL for 6 d. Dentin slices were then stained by toluidine blue and observed under a microscope (model BZ-9000; Keyence Co.).

Analysis of skeletal morphology. Bcl6$^{-/-}$, DKO, and control littermates were necropsied 16 d after birth. Hindlimbs were removed, fixed with 70% ethanol, and subjected to dual-energy x-ray absorptiometry analysis to measure bone mineral density and for bone-histomorphometric analysis. Female 8-wk-old Blimp1 cKO mice and control littermates were administered intraperitoneal injections of 16 mg/kg calcein (Dojindo Co.) at 6 and 1 d before sacrifice to evaluate bone formation rate. Hindlimbs were removed and analyzed as described above.

ELISA. Serum levels of osteocalcin and C-terminal telopeptides of type I collagen (CTx) were measured by the Mouse Osteocalcin EIA kit (Biomedical Technologies Inc.) and RatLaps EIA (Immunodiagnostics Systems Ltd.), respectively. Assays were undertaken following the manufacturers' instructions.

Real-time PCR analysis. Total RNAs were isolated from BM cultures by TRIzol reagent (Invitrogen). After denaturation of total RNAs at 70°C for 5 min, cDNAs were synthesized from total RNAs using oligo(dT) primer and reverse transcription (Wako Pure Chemicals Industries). Real-time PCR was performed using SYBR Premix ExTaq II (Takara Bio Inc.) with the DICE Thermal cycler (Takara Bio Inc.), according to the manufacturer's instructions. Samples were matched to a standard curve generated by amplifying serially diluted products using the same PCR reactions. *β-actin* expression served as an internal control. Primer sequences were as follows: *β-actin* forward: 5′-TGAGAGGGAAATCGTGCGTGAC-3′; *β-actin* reverse: 5′-AAGAAGGAAGGCTGGAAAAGAG-3′; *Bcl6* forward: 5′-AGACGCACAGTGACAAACCATACAA-3′; *Bcl6* reverse: 5′-GCTCCACAAATGTTACAGCGATAGG-3′; *Blimp1* forward: 5′-TTCTTGTGTGGTATTGTCGGGACTT-3′; *Blimp1* reverse: 5′-TTGGGGACACTCTTTGGGTAGAGTT-3′; *Ctsk* forward: 5′-ACGGAGGCATTGACTCTGAAGATG-3′; *Ctsk* reverse: 5′-GGAAGCACCAACGAGAGGAGAAAT-3′; *DC-STAMP* forward: 5′-TCCTCCATGAACAAACAGTTCCAA-3′; *DC-STAMP* reverse: 5′-AGACGTGGTTTAGGAATGCAGCTC-3′; *NFATc1* forward: 5′-CAAGTCTCACCACAGGGCTCACTA-3′; *NFATc1* reverse: 5′-GCGTGAGAGGTTCATTCTCCAAGT-3′; *type I collagen* forward: 5′-CCTGGTAAAGATGGTGCC-3′; *type I collagen* reverse: 5′-CACCAGGTTCACCTTTCGCACC-3′; *osteocalcin* forward: 5′-TAGCAGACACCATGAGGACCCT-3′; *osteocalcin* reverse: 5′-TGGACATGAAGGCTTTGTCAGA-3′.

Immunofluoresence. Cells were fixed with 4% paraformaldehyde (Wako Pure Chemical Industries) in PBS solution for 15 min at room temperature. After washing to remove fixation solution, cells were permeabilized in PBS containing 0.1% Triton X-100 for 10 min at room temperature and then washed. Nonspecific antibody binding was blocked by treatment with 5% BSA (Sigma-Aldrich Co.) in PBS. Cells were then stained with anti-Bcl6 antibody (1:50 dilution, N-3; Santa Cruz Biotechnology, Inc.) at 4°C overnight, washed with PBS and stained with Alexa Fluor 546–conjugated anti-rabbit IgG antibody (1:200 dilution) for 1 h at room temperature. Cells were washed to remove secondary antibody and incubated with DAPI solution (Dojindo Co.; 1:5,000) for nuclear staining, followed by microscopic observation (model BZ-9000; Keyence Co).

Immunoblotting analysis. Whole-cell lysates were prepared from BM cultures using RIPA buffer (1% Triton X-100, 1% sodium deoxycholate, 0.1% SDS, 150 mM NaCl, 10 mM Tris-HCl, pH 7.5, 5 mM EDTA, and a protease inhibitor cocktail; Sigma-Aldrich). Equivalent amounts of protein were separated by SDS-PAGE and transferred to a PVDF membrane (Millipore). Proteins were detected using the following antibodies: anti-NFATc1 (7A6), anti-Blimp1 (6D3), anti-Bcl6 (N-3) (Santa Cruz Biotechnology, Inc.), and anti-actin (A2066; Sigma-Aldrich).

EMSA. Nuclear extracts were prepared from COS7 cells transfected with pCAG-HA-Blimp1 or pCAG. Each extract was incubated for 30 min on ice with a [^{32}P]labeled probe in binding buffer (10 mM Tris-HCl, pH 7.9, 50 mM NaCl, 0.5 mM EDTA, 1 mM DTT, and 10% glycerol) containing 2 μg of poly(dI-dC), KCl, and BSA. Complexes were separated on 5% polyacrylamide gels in TGE buffer (25 mM Tris-HCl, 190 mM glycine, and 1 mM EDTA). The Bcl6 probe corresponding to a putative Blimp1 binding site in the *Bcl6* gene was 5′-AGGTTTCATAGGAAGTGAAAACCCTGCTAT-3′. A mutated probe (underlined residues) served as a negative control (Bcl6mut probe; 5′-AGGTTTCATAGGAAGTTAGAACCCTGCTAT-3′). After electrophoresis, gels were dried and exposed to the imaging plate, and signals were analyzed using ImageGauge software on the BAS2000 image analyzer (Fuji Film Co.).

ChIP. ChIP was performed on osteoclasts. M-CSF–induced BMMs were cultured on 100-mm type I collagen-coated culture dishes (Asahi Glass Co.) with M-CSF and recombinant RANKL for the indicated time periods, and then subjected to ChIP analysis using the ChIP-IT Enzymatic kit (ActivMotif Inc.), according to the manufacturer's instructions. Immunoprecipitation was performed using anti-NFATc1 (7A6), anti-Bcl6 (N-3), and anti-Blimp1 (C14A4; Cell Signaling Technology). DNA was purified by QIAquick PCR purification kit (QIAGEN) and analyzed using primers corresponding to the following promoters: *NFATc1*-P1 promoter, 5′-CCGGGACGCCCATGCAATCTGTTAGTAATT-3′ (sense) and 5′-GCGGGTGCCCTGAGAAAGCTACTCTCCCTT-3′ (antisense); the *DC-STAMP* promoter, 5′-GGGGGTCCTCATTTCTACAACTCAT-3′

Published April 5, 2010

(sense) and 5′-GCCACATCACCCTGAATCAATCTT-3′ (antisense); the *Ctsk* promoter, 5′-CCTTAAACTGGCTCCTGTCAAAGA-3′ (sense) and 5′-CCCTTCTTCAGAAGCCCTGTAAT-3′ (antisense); *NFATc2* promoter, 5′-TTATCAGGGAGCACTGCCCATCTCCGCTTT-3′ (sense) and 5′-CGGTCTGGCCTGAGCGACAGGCCCAGACAA-3′ (antisense); and *Bcl6* promoter, 5′-CAGCCACCCTGAGTTTACAA-3′ (sense) and 5′-CGTTCCAGCACTGTTTTGAA-3′ (antisense).

Microarray analysis. BM cells were isolated from 8-wk-old mouse and cultured in the presence of M-CSF for 3 d. M-CSF–dependent adherent cells were harvested and cultured with M-CSF alone for macrophages and M-CSF plus RANKL for osteoclasts, respectively. After 6 days of cultivation, total RNA was isolated and microarray analysis was undertaken using GeneChip Mouse Genome 430 2.0 Array (Affymetrix). Data were analyzed using GeneChip Operating Software and deposited in Minimum Information about a Microarray Experiment compliant in Gene Expression Omnibus (GEO accession no. GSE20850).

Online supplemental material. Fig. S1 shows that *Bcl6* is transcriptionally repressed by RANKL. Fig. S2 shows bone parameters of $Bcl6^{+/-}$ and $Bcl6^{-/-}$ mice. Fig. S3 shows proliferation and apoptosis of osteoclast precursors from $Bcl6^{+/-}$ and $Bcl6^{-/-}$ mice. Fig. S4 shows Blimp1 expression in osteoclasts. Fig. S5 shows that Blimp1 binds to the Bcl6 promoter. Fig. S6 shows normal osteoblastic differentiation in Blimp1 cKO cells. Fig. S7 shows proliferation and apoptosis of osteoclast precursors from Blimp1 cKO and control mice. Fig. S8 shows immune cell populations in spleens of Blimp1 cKO and control mice. Fig. S9 shows dysregulation of Bcl6 in Blimp1 cKO BMM. Online supplemental material is available at http://www.jem.org/cgi/content/full/jem.20091957/DC1.

We thank Y. Sato for technical support. We thank Prof. T. Kitamura (University of Tokyo) and Prof. A. Tarakhovsky (Rockefeller University) for providing retroviral vectors and $Blimp1^{+/-}$ mice, respectively.

T. Miyamoto was supported by a grant-in-aid for Young Scientists, Precursory Research for Embryonic Science and Technology (PREST), the Uehara memorial foundation, Takeda Science Foundation, The Nakatomi Foundation, and Keio Kanrinmaru project, Japan. Y. Miyauchi was supported by a grant-in-aid for Young Scientists.

The authors have no conflicting financial interests.

Submitted: 8 September 2009
Accepted: 10 March 2010

REFERENCES

Anderson, D.M., E. Maraskovsky, W.L. Billingsley, W.C. Dougall, M.E. Tometsko, E.R. Roux, M.C. Teepe, R.F. DuBose, D. Cosman, and L. Galibert. 1997. A homologue of the TNF receptor and its ligand enhance T-cell growth and dendritic-cell function. *Nature.* 390:175–179. doi:10.1038/36593

Asagiri, M., K. Sato, T. Usami, S. Ochi, H. Nishina, H. Yoshida, I. Morita, E.F. Wagner, T.W. Mak, E. Serfling, and H. Takayanagi. 2005. Autoamplification of NFATc1 expression determines its essential role in bone homeostasis. *J. Exp. Med.* 202:1261–1269. doi:10.1084/jem.20051150

Baron, B.W., J. Anastasi, M.J. Thirman, Y. Furukawa, S. Fears, D.C. Kim, F. Simone, M. Birkenbach, A. Montag, A. Sadhu, et al. 2002. The human programmed cell death-2 (PDCD2) gene is a target of BCL6 repression: implications for a role of BCL6 in the down-regulation of apoptosis. *Proc. Natl. Acad. Sci. USA.* 99:2860–2865. doi:10.1073/pnas.042702599

Cimmino, L., G.A. Martins, J. Liao, E. Magnusdottir, G. Grunig, R.K. Perez, and K.L. Calame. 2008. Blimp-1 attenuates Th1 differentiation by repression of ifng, tbx21, and bcl6 gene expression. *J. Immunol.* 181:2338–2347.

Dent, A.L., J. Hu-Li, W.E. Paul, and L.M. Staudt. 1998. T helper type 2 inflammatory disease in the absence of interleukin 4 and transcription factor STAT6. *Proc. Natl. Acad. Sci. USA.* 95:13823–13828. doi:10.1073/pnas.95.23.13823

Dougall, W.C., M. Glaccum, K. Charrier, K. Rohrbach, K. Brasel, T. De Smedt, E. Daro, J. Smith, M.E. Tometsko, C.R. Maliszewski, et al. 1999. RANK is essential for osteoclast and lymph node development. *Genes Dev.* 13:2412–2424. doi:10.1101/gad.13.18.2412

Fukuda, T., T. Yoshida, S. Okada, M. Hatano, T. Miki, K. Ishibashi, S. Okabe, H. Koseki, S. Hirosawa, M. Taniguchi, et al. 1997. Disruption of the Bcl6 gene results in an impaired germinal center formation. *J. Exp. Med.* 186:439–448. doi:10.1084/jem.186.3.439

Ichii, H., A. Sakamoto, Y. Kuroda, and T. Tokuhisa. 2004. Bcl6 acts as an amplifier for the generation and proliferative capacity of central memory CD8+ T cells. *J. Immunol.* 173:883–891.

Iwamoto, K., T. Miyamoto, N. Hosogane, I. Hamaguchi, M. Takami, K. Takagi, and T. Suda. 2004. Dimer formation of receptor activator of nuclear factor kappa B induces incomplete osteoclast formation. *Biochem. Biophys. Res. Commun.* 325:229–234. doi:10.1016/j.bbrc.2004.10.024

Iwasawa, M., T. Miyazaki, Y. Nagase, T. Akiyama, Y. Kadono, M. Nakamura, Y. Oshima, T. Yasui, T. Matsumoto, T. Nakamura, et al. 2009. The antiapoptotic protein Bcl-xL negatively regulates the bone-resorbing activity of osteoclasts in mice. *J. Clin. Invest.* 119:3149–3159.

John, S.A., and L.A. Garrett-Sinha. 2009. Blimp1: a conserved transcriptional repressor critical for differentiation of many tissues. *Exp. Cell Res.* 315:1077–1084. doi:10.1016/j.yexcr.2008.11.015

Kallies, A., E.D. Hawkins, G.T. Belz, D. Metcalf, M. Hommel, L.M. Corcoran, P.D. Hodgkin, and S.L. Nutt. 2006. Transcriptional repressor Blimp-1 is essential for T cell homeostasis and self-tolerance. *Nat. Immunol.* 7:466–474. doi:10.1038/ni1321

Karsenty, G., and E.F. Wagner. 2002. Reaching a genetic and molecular understanding of skeletal development. *Dev. Cell.* 2:389–406. doi:10.1016/S1534-5807(02)00157-0

Keller, A.D., and T. Maniatis. 1991. Identification and characterization of a novel repressor of beta-interferon gene expression. *Genes Dev.* 5:868–879. doi:10.1101/gad.5.5.868

Kim, K., J.H. Kim, J. Lee, H.M. Jin, H. Kook, K.K. Kim, S.Y. Lee, and N. Kim. 2007. MafB negatively regulates RANKL-mediated osteoclast differentiation. *Blood.* 109:3253–3259. doi:10.1182/blood-2006-09-048249

Koga, T., M. Inui, K. Inoue, S. Kim, A. Suematsu, E. Kobayashi, T. Iwata, H. Ohnishi, T. Matozaki, T. Kodama, et al. 2004. Costimulatory signals mediated by the ITAM motif cooperate with RANKL for bone homeostasis. *Nature.* 428:758–763. doi:10.1038/nature02444

Koga, T., Y. Matsui, M. Asagiri, T. Kodama, B. de Crombrugghe, K. Nakashima, and H. Takayanagi. 2005. NFAT and Osterix cooperatively regulate bone formation. *Nat. Med.* 11:880–885. doi:10.1038/nm1270

Kong, Y.Y., H. Yoshida, I. Sarosi, H.L. Tan, E. Timms, C. Capparelli, S. Morony, A.J. Oliveira-dos-Santos, G. Van, A. Itie, et al. 1999. OPGL is a key regulator of osteoclastogenesis, lymphocyte development and lymph-node organogenesis. *Nature.* 397:315–323. doi:10.1038/16852

Kurimoto, K., Y. Yabuta, Y. Ohinata, M. Shigeta, K. Yamanaka, and M. Saitou. 2008. Complex genome-wide transcription dynamics orchestrated by Blimp1 for the specification of the germ cell lineage in mice. *Genes Dev.* 22:1617–1635. doi:10.1101/gad.1649908

Kusam, S., L.M. Toney, H. Sato, and A.L. Dent. 2003. Inhibition of Th2 differentiation and GATA-3 expression by BCL-6. *J. Immunol.* 170:2435–2441.

Lee, J., K. Kim, J.H. Kim, H.M. Jin, H.K. Choi, S.H. Lee, H. Kook, K.K. Kim, Y. Yokota, S.Y. Lee, et al. 2006. Id helix-loop-helix proteins negatively regulate TRANCE-mediated osteoclast differentiation. *Blood.* 107:2686–2693. doi:10.1182/blood-2005-07-2798

Li, C.Y., K.J. Jepsen, R.J. Majeska, J. Zhang, R. Ni, B.D. Gelb, and M.B. Schaffler. 2006. Mice lacking cathepsin K maintain bone remodeling but develop bone fragility despite high bone mass. *J. Bone Miner. Res.* 21:865–875. doi:10.1359/jbmr.060313

Martins, G.A., L. Cimmino, M. Shapiro-Shelef, M. Szabolcs, A. Herron, E. Magnusdottir, and K. Calame. 2006. Transcriptional repressor Blimp-1 regulates T cell homeostasis and function. *Nat. Immunol.* 7:457–465. doi:10.1038/ni1320

Matsumoto, M., M. Kogawa, S. Wada, H. Takayanagi, M. Tsujimoto, S. Katayama, K. Hisatake, and Y. Nogi. 2004. Essential role of p38 mitogen-activated protein kinase in cathepsin K gene expression during

Published April 5, 2010

JEM

osteoclastogenesis through association of NFATc1 and PU.1. *J. Biol. Chem.* 279:45969–45979. doi:10.1074/jbc.M408795200

Miyamoto, T., F. Arai, O. Ohneda, K. Takagi, D.M. Anderson, and T. Suda. 2000. An adherent condition is required for formation of multinuclear osteoclasts in the presence of macrophage colony-stimulating factor and receptor activator of nuclear factor kappa B ligand. *Blood.* 96:4335–4343.

Nakamura, T., Y. Imai, T. Matsumoto, S. Sato, K. Takeuchi, K. Igarashi, Y. Harada, Y. Azuma, A. Krust, Y. Yamamoto, et al. 2007. Estrogen prevents bone loss via estrogen receptor alpha and induction of Fas ligand in osteoclasts. *Cell.* 130:811–823. doi:10.1016/j.cell.2007.07.025

Nakashima, T., and H. Takayanagi. 2008. The dynamic interplay between osteoclasts and the immune system. *Arch. Biochem. Biophys.* 473:166–171. doi:10.1016/j.abb.2008.04.004

Ng, D., N. Thakker, C.M. Corcoran, D. Donnai, R. Perveen, A. Schneider, D.W. Hadley, C. Tifft, L. Zhang, A.O. Wilkie, et al. 2004. Oculofaciocardiodental and Lenz microphthalmia syndromes result from distinct classes of mutations in BCOR. *Nat. Genet.* 36:411–416. doi:10.1038/ng1321

Northrop, J.P., S.N. Ho, L. Chen, D.J. Thomas, L.A. Timmerman, G.P. Nolan, A. Admon, and G.R. Crabtree. 1994. NF-AT components define a family of transcription factors targeted in T-cell activation. *Nature.* 369:497–502. doi:10.1038/369497a0

Ohinata, Y., B. Payer, D. O'Carroll, K. Ancelin, Y. Ono, M. Sano, S.C. Barton, T. Obukhanych, M. Nussenzweig, A. Tarakhovsky, et al. 2005. Blimp1 is a critical determinant of the germ cell lineage in mice. *Nature.* 436:207–213. doi:10.1038/nature03813

Ohinata, Y., H. Ohta, M. Shigeta, K. Yamanaka, T. Wakayama, and M. Saitou. 2009. A signaling principle for the specification of the germ cell lineage in mice. *Cell.* 137:571–584. doi:10.1016/j.cell.2009.03.014

Ohno, H. 2006. Pathogenetic and clinical implications of non-immunoglobulin; BCL6 translocations in B-cell non-Hodgkin's lymphoma. *J. Clin. Exp. Hematop.* 46:43–53. doi:10.3960/jslrt.46.43

Rodan, G.A., and T.J. Martin. 2000. Therapeutic approaches to bone diseases. *Science.* 289:1508–1514. doi:10.1126/science.289.5484.1508

Sato, K., A. Suematsu, T. Nakashima, S. Takemoto-Kimura, K. Aoki, Y. Morishita, H. Asahara, K. Ohya, A. Yamaguchi, T. Takai, et al. 2006. Regulation of osteoclast differentiation and function by the CaMK-CREB pathway. *Nat. Med.* 12:1410–1416. doi:10.1038/nm1515

Sawatani, Y., T. Miyamoto, S. Nagai, M. Maruya, J. Imai, K. Miyamoto, N. Fujita, K. Ninomiya, T. Suzuki, R. Iwasaki, et al. 2008. The role of DC-STAMP in maintenance of immune tolerance through regulation of dendritic cell function. *Int. Immunol.* 20:1259–1268. doi:10.1093/intimm/dxn082

Shaffer, A.L., K.I. Lin, T.C. Kuo, X. Yu, E.M. Hurt, A. Rosenwald, J.M. Giltnane, L. Yang, H. Zhao, K. Calame, and L.M. Staudt. 2002. Blimp-1 orchestrates plasma cell differentiation by extinguishing the mature B cell gene expression program. *Immunity.* 17:51–62. doi:10.1016/S1074-7613(02)00335-7

Shapiro-Shelef, M., and K. Calame. 2005. Regulation of plasma-cell development. *Nat. Rev. Immunol.* 5:230–242. doi:10.1038/nri1572

Shinohara, M., T. Koga, K. Okamoto, S. Sakaguchi, K. Arai, H. Yasuda, T. Takai, T. Kodama, T. Morio, R.S. Geha, et al. 2008. Tyrosine kinases Btk and Tec regulate osteoclast differentiation by linking RANK and ITAM signals. *Cell.* 132:794–806. doi:10.1016/j.cell.2007.12.037

Takayanagi, H., S. Kim, T. Koga, H. Nishina, M. Isshiki, H. Yoshida, A. Saiura, M. Isobe, T. Yokochi, J. Inoue, et al. 2002. Induction and activation of the transcription factor NFATc1 (NFAT2) integrate RANKL signaling in terminal differentiation of osteoclasts. *Dev. Cell.* 3:889–901. doi:10.1016/S1534-5807(02)00369-6

Turner, C.A. Jr., D.H. Mack, and M.M. Davis. 1994. Blimp-1, a novel zinc finger-containing protein that can drive the maturation of B lymphocytes into immunoglobulin-secreting cells. *Cell.* 77:297–306. doi:10.1016/0092-8674(94)90321-2

Vincent, S.D., N.R. Dunn, R. Sciammas, M. Shapiro-Shalef, M.M. Davis, K. Calame, E.K. Bikoff, and E.J. Robertson. 2005. The zinc finger transcriptional repressor Blimp1/Prdm1 is dispensable for early axis formation but is required for specification of primordial germ cells in the mouse. *Development.* 132:1315–1325. doi:10.1242/dev.01711

Yagi, M., T. Miyamoto, Y. Sawatani, K. Iwamoto, N. Hosogane, N. Fujita, K. Morita, K. Ninomiya, T. Suzuki, K. Miyamoto, et al. 2005. DC-STAMP is essential for cell-cell fusion in osteoclasts and foreign body giant cells. *J. Exp. Med.* 202:345–351. doi:10.1084/jem.20050645

Yagi, M., K. Ninomiya, N. Fujita, T. Suzuki, R. Iwasaki, K. Morita, N. Hosogane, K. Matsuo, Y. Toyama, T. Suda, and T. Miyamoto. 2007. Induction of DC-STAMP by alternative activation and downstream signaling mechanisms. *J. Bone Miner. Res.* 22:992–1001. doi:10.1359/jbmr.070401

Zhao, B., M. Takami, A. Yamada, X. Wang, T. Koga, X. Hu, T. Tamura, K. Ozato, Y. Choi, L.B. Ivashkiv, et al. 2009. Interferon regulatory factor-8 regulates bone metabolism by suppressing osteoclastogenesis. *Nat. Med.* 15:1066–1071. doi:10.1038/nm.2007

J Neurosurg Spine 13:246–252, 2010

Ball tip technique for thoracic pedicle screw placement in patients with adolescent idiopathic scoliosis

Technical note

Kota Watanabe, M.D.,[1] Morio Matsumoto, M.D.,[2] Takashi Tsuji, M.D.,[2] Ken Ishii, M.D.,[2] Hironari Takaishi, M.D.,[2] Masaya Nakamura, M.D.,[2] Yoshiaki Toyama, M.D.,[2] and Kazuhiro Chiba, M.D.[2]

Departments of [1]Advanced Treatment for Spine and Spinal Cord Disorders and [2]Orthopedic Surgery, Keio University School of Medicine, Tokyo, Japan

Object. The aim in this study was to evaluate the efficacy of the ball tip technique in placing thoracic pedicle screws (TPSs), as compared with the conventional freehand technique, in both a cadaveric study and a clinical study of patients with adolescent idiopathic scoliosis. Although posterior spinal surgery using TPSs has been widely applied, these screws are associated with the potential risk of vascular, pulmonary, or neurological complications. To further enhance the accuracy and safety of TPS placement, the authors developed the ball tip technique.

Methods. After creating an appropriate starting point for probe insertion, a specially designed ball tip probe consisting of a ball-shaped tip with a flexible metal shaft is used to make a guide hole into the pedicle. Holding the probe with the fingertips while using an appropriate amount of pressure or by tapping it gently and continuously with a hammer, one can safely insert the ball tip probe into the cancellous channel in the pedicle.

In a cadaveric study, 5 spine fellows with similar levels of experience in placing TPSs applied the ball tip or the conventional technique to place screws in 5 cadavers with no spinal deformities. The incidence of misplaced screws was evaluated by dissecting the spines. In a clinical study, 40 patients with adolescent idiopathic scoliosis underwent posterior surgery with TPS placement via the ball tip or conventional technique (20 patients in each treatment group). The accuracy of the TPS placements was evaluated on postoperative axial CT scanning.

Results. In the cadaveric study, 100 TPSs were evaluated, and the incidence of misplaced screws was 14% in the ball tip group and 34% in the conventional group ($p = 0.0192$). In the clinical study, 574 TPSs were evaluated. One hundred seventy-one intrapedicular screws (67%) were recognized in the conventional group and 288 (90%) in the ball tip group ($p < 0.01$). In the conventional and ball tip groups, the respective numbers of TPSs with a pedicle breach of ≤ 2 mm were 20 (8%) and 15 (5%), those with a pedicle breach of > 2 mm were 32 (13%) and 9 (3%; $p < 0.01$), and those located in the costovertebral joints were 32 (13%) and 7 (2%).

Conclusions. In both cadaveric and clinical studies the ball tip technique enhanced the accuracy of TPS placement as compared with the conventional freehand technique. Thus, the ball tip technique is useful for the accurate and safe placement of TPSs in deformed spines. *(DOI: 10.3171/2010.3.SPINE09497)*

Key Words • **adolescent idiopathic scoliosis** • **ball tip technique** • **thoracic pedicle screw** • **posterior correction surgery**

Posterior spinal correction surgery using TPSs has gained popularity among spine surgeons for the treatment of spinal deformity, replacing hook and wire constructs because mechanically strong TPS constructs provide 3D correction of the deformity and eliminate the need for postoperative bracing.[5,6,8,12] However, TPSs are associated with the potential risks of vascular, pulmonary, or neurological injuries, which can result in catastrophic sequelae.[2,10] A variety of techniques have been developed for the safe and accurate placement of these screws, including "anatomical" techniques such as the freehand technique,[7] open-lamina technique,[13] mini-laminotomy technique,[4] and the insertion of guide pins at pedicle entry points.[11] Computer-generated imaging techniques have also been proposed as a means of fur-

Abbreviations used in this paper: AIS = adolescent idiopathic scoliosis; TPS = thoracic pedicle screw.

ther minimizing the misplacement of TPSs.[1–3,9] Although computer-generated imaging techniques have decreased the incidence of screw misplacement, their use requires a longer operative time, which can increase intraoperative blood loss and the chance of wound infection.

Since October 2006, we have been utilizing the ball tip technique rather than the freehand technique for TPS placement during posterior spinal correction surgery to enhance the accuracy and safety of screw insertion without requiring a prolonged surgical time and costly special equipment. In the ball tip technique, a specially designed flexible "ball tip probe" (Fig. 1) is used for the placement of TPSs. The purpose of our study was to confirm whether the ball tip technique enhances the accuracy of TPS placement compared with the conventional freehand technique in both cadaveric studies and clinical studies in patients with AIS.

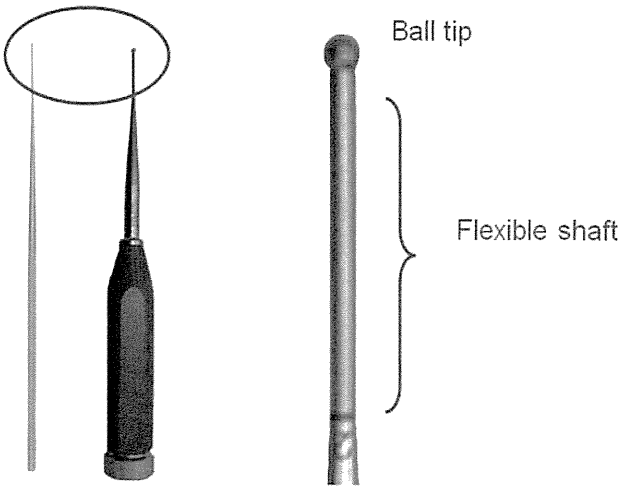

FIG. 1. Illustration of the ball tip probe, which consists of a ball-shaped metal tip with a metal flexible shaft. It is used to create a guide hole in the ball tip technique.

Methods

Thoracic Pedicle Screw Placement Technique

Ball Tip Technique. First, the posterior elements including the spinous processes, laminae, facets, and transverse processes are meticulously exposed. The starting points for TPS placement at each thoracic vertebra are identical to those proposed by Kim et al.[7] A 5-mm high-speed bur is used to remove the cortical bone of the dorsal lamina at the appropriate starting points approximately 3 mm in depth and then to expose the cancellous bone suggesting entrance at the base of the pedicle. Next, a specially designed ball tip probe is used to make a guide hole through the pedicle into the vertebral body. The ball tip probe consists of a ball-shaped metal tip with a flexible metal shaft (Medtronic Sofamor Danek; Fig. 1). It is held with the fingertips and gently pushed into the cancellous channel of the pedicle (Fig. 2). The ventral pressure of the ball tip probe is slightly less than is needed when inserting a rigid thoracic pedicle probe. If the cancellous channel is wide enough, the tip of the probe is smoothly advanced into the pedicle. If the cancellous channel is narrowed or if the tip of the probe makes contact with the cortical bone of the pedicle, a slight resistance against the probe will be encountered. In that case, the probe can be very gently tapped with a hammer (Fig. 3). Gentle tapping enables the ball tip to slip along the cortical wall into the cancellous channel of the pedicle (Fig. 4). Once the tip of the probe passes beyond the isthmus of the pedicle, which is recognized by a loss of resistance, the probe easily passes into the vertebral body. The probe is advanced until its tip hits the anterior cortex of the vertebral body. One should feel the probe penetrating the cancellous bone for the entire length of the pedicle and the vertebral body. Any sudden advancement of the ball tip probe suggests penetration of the pedicle or vertebral body. A gearshift probe (Medtronic Sofamor Danek; Fig. 5) is used to widen the guide hole. Next, a pedicle sounding device is used to check whether the pedicle walls have been breached. The TPS length is typically 5 mm less than the maximal probed depth, as determined by directly measuring the pedicle length using a pedicle sounder. The TPS diameter is predetermined based on preoperative CT studies. For patients with AIS, the typical screw diameter is 5.5 mm in the upper and midthoracic regions and 5.5–6.5 mm in the lower thoracic regions (T10–12). The pedicle is tapped using a tap device that is 1 mm smaller than the actual TPS diameter. After a recheck for pedicle perforation using the pedicle sounder, the TPS is placed through the pedicle into the vertebral body (Fig. 6).

Conventional Freehand Technique. Basically, the conventional freehand technique in this study corresponds to the freehand technique described by Kim et al.[7] In the conventional technique, the gearshift probe (Fig. 5) is used to create the guide hole after identification of the starting point. The conventional technique is essentially the same as the ball tip technique except for the use of the ball tip probe (Fig. 1) in creating the guide hole.

Cadaveric Study

Five cadavers (2 male and 3 female) were used in the cadaveric study. The average age at the time of death was 88.2 years (range 78–95 years), and the average height was 155 cm (range 145–160 cm). No evidence of congenital or developmental spinal malformations was found in any of the cadavers. All the cadavers had various degrees of age-related osteoporosis and degenerative changes.

Five spine fellows who had completed a similar training program in spine surgery conducted the cadaveric study; none of them had any experience in TPS placement. The cadavers were placed prone, and a standard midline posterior approach was used to expose the posterior elements. Each of the 5 cadavers was randomly assigned to a fellow. In each cadaver, the conventional technique and the ball tip technique were used for placement of the TPSs. Before starting screw placement, the fellows attended a senior surgeon's lecture regarding anatomy of the thoracic vertebra and the procedure for screw placement, especially how to find an appropriate starting point for TPS insertion at different thoracic levels. Exercises

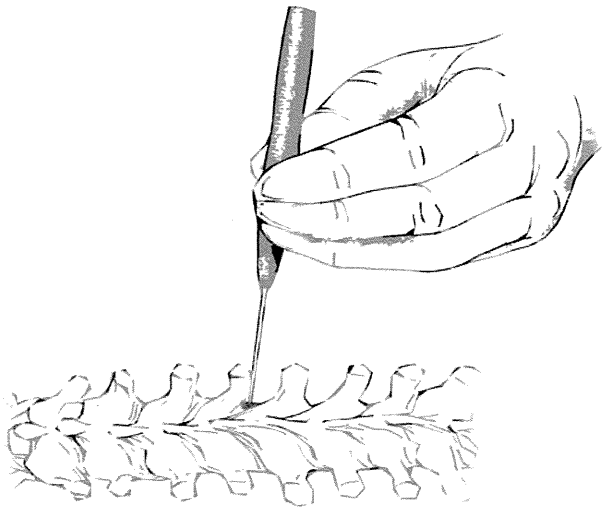

FIG. 2. Illustration demonstrating the ball tip technique (probe insertion). The ball tip probe is used to make a guide hole in the pedicle after the creation of a cortical breach at an appropriate starting point. Holding it with the fingertips, the probe is inserted into the pedicle with an appropriate amount of ventral pressure.

for handling the screw-placing devices, such as the ball tip and the gearshift probes, were performed utilizing lumbar pedicle screw placement.

During the actual TPS placements, starting points were identified by the senior surgeon if the fellow was unable to locate the correct position. The TPSs were placed from T-3 to T-12 in all the cadavers (Fig. 7). The ball tip technique was performed before the conventional technique using 1 side of the spine; then the conventional technique was applied on the opposite side. The ball tip technique was performed on the left side in 3 cadavers and on the right side in 2. Once all TPS placements had been completed, the cadaveric specimens were dissected to evaluate the accuracy of screw placements. The presence or absence of a pedicle perforation and its direction—medial or lateral—were judged by 2 independent observers.

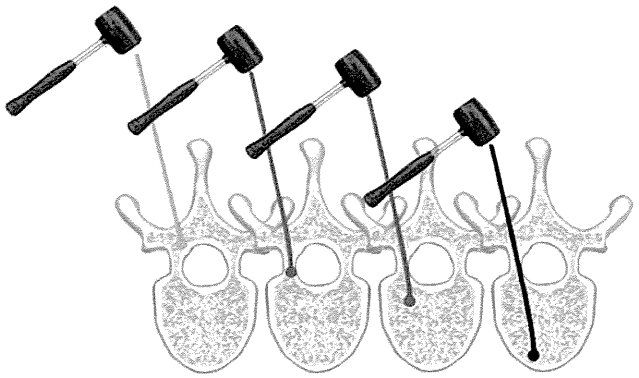

FIG. 3. Illustration depicting the ball tip technique with hammer tapping. If the probe encounters slight resistance, it can be tapped very gently and continuously by using a hammer.

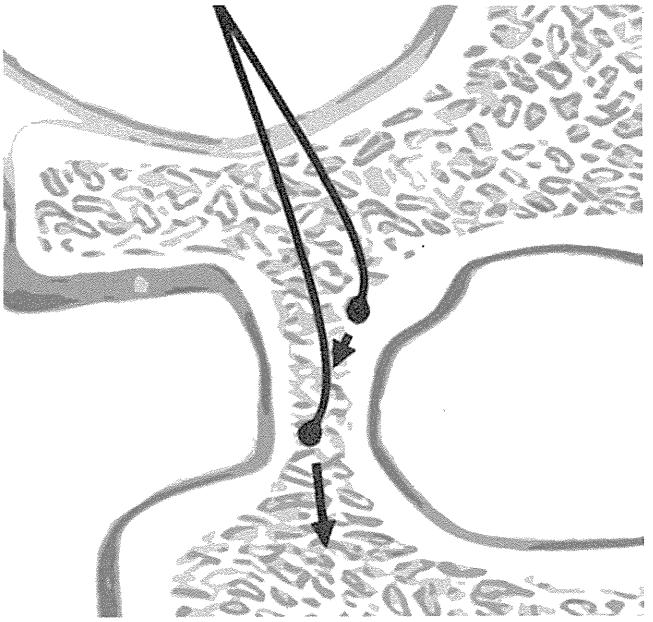

FIG. 4. Drawing showing the behavior of a ball tip in a pedicle. When the ball tip reaches the cortical wall of the pedicle, the shaft of the probe bends slightly against the inner cortical wall and the ball tip slips along the surface of the cortical bone without penetrating it; the tip then proceeds into the cancellous vertebral bone, where the resistance is much smaller.

Medial perforation was determined after a laminectomy and lateral perforation after rib disarticulations at every level. Pedicle screws without any cortical perforations were considered to be successfully placed. The accuracies of TPS placements using the conventional technique versus the ball tip technique were then compared.

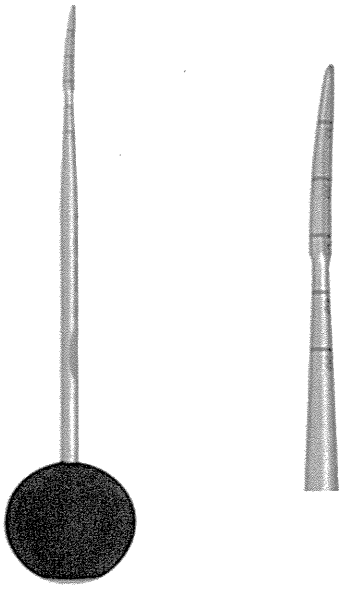

FIG. 5. Illustration depicting a gearshift probe: a 2-mm, blunt-tipped, slightly curved probe. This probe is used to widen the guide hole made by the ball tip probe. The gearshift probe is also used to create the guide hole in the conventional technique.

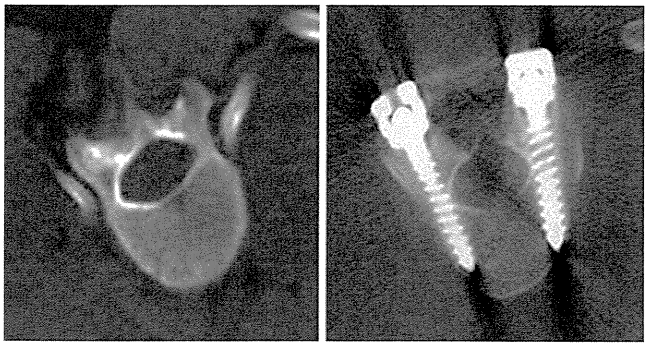

FIG. 6. A preoperative CT scan **(left)** showing a severely rotated T-10 vertebra with narrowed pedicles. A postoperative CT **(right)** demonstrating 5.5 × 35–mm TPSs placed into the pedicles. These TPSs were in an intrapedicular position.

Clinical Study in Patients With AIS

Forty patients with AIS who had been treated using only TPSs and lumbar pedicle screws were included in this study (Table 1). All patients had a main thoracic curve (Lenke Type 1, 21 cases; Type 2, 14 cases; and Type 4, 5 cases). Patients were divided into 2 treatment groups: a ball tip group and a conventional group. The ball tip group consisted of 20 consecutive patients who underwent posterior correction surgery using the ball tip technique between November 2006 and December 2007. There were 2 male and 18 female patients, with a mean age of 14.5 ± 3.1 years (range 9–22 years) at the time of surgery. The conventional group consisted of 20 consecutive patients who underwent posterior correction surgery using the conventional freehand technique[7] for TPS placement between December 2004 and October 2006. These 20 patients were the most recent cases treated using the conventional technique before the introduction of the ball tip technique. There were 3 male and 17 female patients, with a mean age of 13.4 ± 3.3 years (range 9–22 years) at the time of surgery. The mean Cobb angle of the main thoracic curve was 63.9 ± 14.6° (range 34–105°) in the ball tip group and 60.3 ± 5.3° (range 47–90°) in the conventional group. No significant differences in patient age at the time of surgery or the Cobb angle of the main thoracic curve were observed between the 2 groups.

Pedicle Screw Placement Planning in Patients With AIS

Basically, the TPSs were placed at the most cranial and the most caudal 2 vertebrae in the fusion area. On the concave side, the TPSs were placed in all the pedicles of the main curve. On the convex side, screw placement was occasionally omitted in a few pedicles. Screw placement in both groups was discontinued if pedicle perforations were recognized after several trials. Postoperatively, a retrospective morphological evaluation of these abandoned pedicles was performed using preoperative axial CT scans. The evaluated parameters included the width at the isthmus and the percentage of the cancellous bone width at the isthmus.

Pedicle screw placements on the left side were performed by a single senior spine surgeon, whereas those on the right side were performed by spine fellows under the direct supervision of the senior surgeon. Two spine fellows were involved in the conventional TPS placement and another spine fellow used the ball tip technique during this study.

TABLE 1: Summary of characteristics in the ball tip group and conventional group

Characteristic	Ball Tip Group	Conventional Group
no. of cases	20	20
treatment period	Nov 2006–Dec 2007	Dec 2004–Oct 2006
mean age in yrs (range)	14.5 ± 3.1 (9–22)	13.4 ± 3.3 (9–22)
sex		
M	2	3
F	18	17
Lenke type		
1	11	10
2	6	8
4	3	2
Cobb angle of main thoracic curve in degrees (range)	63.9 ± 14.6 (34–105)	60.3 ± 5 (47–90)

Computed Tomography Analysis

The accuracy of TPS placements was evaluated based on postoperative fine-cut (width of 1.25 mm) CTs in all patients in the clinical study. All thoracic levels were scanned using CT, and the gantry was set parallel to the TPSs. The positions of the screws were classified as follows: intrapedicular, pedicle breach ≤ 2 mm, pedicle breach > 2 mm, and intracostovertebral joints.[2] The direction of the pedicle breach (medial, anterior, or lateral) was also recorded. For screws with a pedicle breach, the maximum distance between the surface of the TPS and the outer cortex of the pedicle was measured using NIH Image software. All CT scans were filtered to minimize the metal artifact. Perforations of the anterior vertebral cortex were measured along the axis of the screw. An independent observer evaluated in a blinded manner the accuracy of TPS placements.

Statistical Analysis

A chi-square test was used to compare the accuracies of the ball tip group with those of the conventional group in both the cadaveric and clinical studies. Statistical significance was defined as $p < 0.05$. Statistical analysis was performed using SPSS, version 10.0 (SPSS, Inc.). Mean values are presented ± SDs.

TABLE 2: Summary of results of cadaveric study

Treatment	No. of Cases				
	Lateral Breach	Medial Breach	Total Breach	Intrapedicle (%)*	Total
ball tip method	4	3	7	43 (86)	50
conventional free-hand method	6	11	17	33 (66)	50

* p = 0.0138 with chi-square test, ball tip method compared with conventional method.

TABLE 3: Positions of TPSs

Parameter	No. of TPSs (%)	
	Conventional Group	Ball Tip Group
intrapedicular*	171 (67.1)	288 (90.3)
pedicle breach of ≤2 mm	20 (7.8)	15 (4.7)
pedicle breach of >2 mm*	32 (12.5)	9 (2.8)
intracostovertebral joint*	32 (12.5)	7 (2.2)
total	255 (100)	319 (100)

* p < 0.01, chi-square test, ball tip group compared with conventional group.

Results

Cadaveric Study

One hundred TPSs placed between T-3 and T-12 bilaterally in 5 cadavers were evaluated (Table 2 and Fig. 7). The incidence of TPS misplacement was 14% in the ball tip group (7 pedicles, 4 lateral, and 3 medial) and 34% in the conventional group (17 pedicles, 6 lateral, and 11 medial). The accuracy of TPS placement was significantly different between the 2 groups (p = 0.0192).

Clinical Study

Pedicle screws were placed in 607 pedicles. In 17 (5.1%) of 336 pedicles in the ball tip group and 16 (5.9%) of 271 pedicles in the conventional group, TPS placement was discontinued because pedicle perforations were recognized after several trials; all these pedicles were located on the concave side of the main curves. A retrospective evaluation of preoperative CT images of these abandoned pedicles in the ball tip group showed that the mean width at the isthmus was 2.8 ± 1.1 mm and the mean percentage of cancellous bone width at the isthmus was 21 ± 28%.

Five hundred seventy-four TPSs were evaluated. The numbers of screws classified as intrapedicular were 171 (67.1%) of the 255 screws placed in the conventional group and 288 (90.3%) of the 319 placed in the ball tip group (Table 3 and Fig. 4). A significant difference in the accuracy of TPS placement was observed between the 2 groups (p < 0.01). Twenty TPSs (7.8%; 7 medial, 9 lateral, and 4 anterior) in the conventional group and 15 (4.7%; 5 medial, 7 lateral, and 3 anterior) in the ball tip group were classified as pedicle breaches of ≤ 2 mm. Thirty-two TPSs (12.5%; 12 medial, 14 lateral, and 6 anterior) in the conventional group and 9 (2.8%; 6 lateral and 3 anterior) in the ball tip group were classified as pedicle breaches of > 2 mm. Thirty-two TPSs (12.5%) in the conventional group and 7 (2.2%) in the ball tip group were located in the costovertebral joints. A significant difference in the percentage of TPSs located in the costovertebral joints was observed between the 2 groups (p < 0.01). No vascular, pulmonary, or neurological injuries caused by TPS placement occurred in either group.

Discussion

Efficacy of Ball Tip Technique

In the clinical study performed in patients with AIS, the accuracy of TPS placement (including intrapedicular plus pedicle breaches of ≤ 2 mm) was 74.9% in the conventional group and 95.0% in the ball tip group. These results indicate that the ball tip technique enhanced the accuracy of TPS placement. In the cadaveric study, the incidences of TPS misplacement were 14% in the ball tip group and 34% in the conventional group. Thus, the ball tip technique was also effective in the cadaveric study, despite the fact that the elderly specimens had very poor bone quality and that the TPS placements were conducted by spine fellows with no previous experience in TPS placement.

In the ball tip technique, the probe is inserted into the cancellous channel of the pedicle either manually or sometimes with gentle tapping using a hammer (Fig. 3). When the ball tip reaches the cortical wall of the pedicle, the shaft of the probe bends slightly against the inner cortical wall and the ball tip slips along the surface of the cortical bone without penetrating it; the tip then proceeds into the cancellous vertebral bone, where the resistance is much smaller (Fig. 4). One of the advantages of the ball tip probe is its flexible shaft, which allows the probe tip to deflect from the cortical bone, especially from the thicker medial cortical bone of the pedicle. Misunderstanding the probe insertion angle, which will increase the risk of pedicle perforation, is more likely to happen in a scoliotic spine since vertebral bodies are always rotated around an apex of the curve. Since the ball tip probe will curve or bend before perforating the cortical bone, the chance of penetrating the pedicles will decrease. In the present study, medial perforations > 2 mm were not found in the ball tip group.

To eliminate a bias in patient selection and surgical techniques, we included the most recent consecutive 20 patients in the conventional group and the earliest consecutive 20 patients in the ball tip group. The TPSs located on the left side of the spine were inserted by the same senior spine surgeon in both groups. Although the

FIG. 7. Photographs demonstrating TPS placement in cadavers. Thoracic pedicle screws were placed from T-3 to T-12 using the ball tip technique and the conventional freehand technique **(left)**. After TPS placement, the presence of medial perforations was evaluated after a laminectomy **(right)**. *Arrows* indicate medial perforations from T-6 to T-8.

TPSs located on the right side of the spine were inserted by different fellows in the 2 groups, all TPS placements were performed under the direct supervision of the senior surgeon.

Limitations of the Ball Tip Technique

The ball tip probe may not work for a well-corticated pedicle or for an extremely small cancellous channel pedicle since the flexible shaft will bend before creating a guide hole in the pedicle. Even using the ball tip technique, TPS placement was discontinued in 17 (5.1%) of 336 pedicles because of repeated perforations by the ball tip probe. The majority of perforations occurred to the lateral side of the pedicles, which might be due to the thicker medial cortex as compared with the lateral cortex. This failure rate is similar to the rate (5.9%) when using the conventional technique. This result indicates that although the ball tip probe enhances the accuracy of TPS placement, there are still some pedicles that cannot accommodate the ball tip probe. An evaluation of preoperative CT axial scans revealed that in such pedicles, the width of the pedicle was relatively narrow (2.7 mm) and the proportion of cancellous bone was relatively low (20%); in other words, these pedicles were slit pedicle channels.

Although we demonstrated the usefulness of the ball tip technique in this study, we must emphasize that it may not be helpful to a surgeon who does not have any experience in placing TPSs. The technique will be more helpful to a surgeon who has had experience in placing TPSs and will help to identify approximate starting points for screw insertions, since a mistake in the identification of a screw starting point can lead to a high rate of missed screw placements even if the ball tip technique is used.

Limitations of This Study

A limitation of this study was that the patients were not randomized for both techniques in the clinical study. Because after several surgeries we felt safe and comfortable with the ball tip technique, we determined that randomization of the patients was not allowed ethically. Instead, we performed the cadaveric study to compare the conventional technique with the ball tip technique at the same time.

Another limitation of the study was that the senior surgeon identified the starting points of the probe insertions if the fellows were unable to determine the correct points. Because the misidentification of starting points would greatly affect the study results, we tried to eliminate the error caused by misidentification of the starting points. Although a lecture about the starting points of probe insertions was given before starting the study, the reliability of inexperienced surgeons in identifying the correct starting points was deemed to be low and varied among them.

Conclusions

In summary, the ball tip technique enhanced the accuracy of TPS placement, compared with the conventional freehand technique, in patients with AIS, in whom TPS placement is regarded to be relatively difficult. An adult cadaveric study also confirmed the efficacy of the ball tip technique. It is expected to be useful for the safe and accurate placement of TPSs in deformed spines.

Disclosure

Dr. Chiba is a consultant for Medtronic Sofamor Danek Japan and Stryker Japan. Drs. Watanabe and Matsumoto are consultants for Medtronic Sofamor Danek Japan.

Author contributions to the study and manuscript preparation include the following. Conception and design: Watanabe, Matsumoto. Acquisition of data: Watanabe. Analysis and interpretation of data: Watanabe. Drafting the article: Watanabe, Matsumoto. Critically revising the article: Watanabe, Tsuji, Ishii, Takaishi, Nakamura. Reviewed final version of the manuscript and approved it for submission: all authors. Statistical analysis: Watanabe. Administrative/technical/material support: Watanabe, Toyama, Chiba. Study supervision: Watanabe, Toyama, Chiba.

References

1. Amiot LP, Lang K, Putzier M, Zippel H, Labelle H: Comparative results between conventional and computer-assisted pedicle screw installation in the thoracic, lumbar, and sacral spine. **Spine 25:**606–614, 2000
2. Belmont PJ Jr, Klemme WR, Dhawan A, Polly DW Jr: In vivo accuracy of thoracic pedicle screws. **Spine 26:**2340–2346, 2001
3. Choi WW, Green BA, Levi AD: Computer-assisted fluoroscopic targeting system for pedicle screw insertion. **Neurosurgery 47:**872–878, 2000
4. Di Silvestre M, Parisini P, Lolli F, Bakaloudis G: Complications of thoracic pedicle screws in scoliosis treatment. **Spine 32:**1655–1661, 2007
5. Gaines RW Jr: The use of pedicle-screw internal fixation for the operative treatment of spinal disorders. **J Bone Joint Surg Am 82:**1458–1476, 2000
6. Hamill CL, Lenke LG, Bridwell KH, Chapman MP, Blanke K, Baldus C: The use of pedicle screw fixation to improve correc-

tion in the lumbar spine of patients with idiopathic scoliosis. Is it warranted? **Spine 21:**1241–1249, 1996
7. Kim YJ, Lenke LG, Bridwell KH, Cho YS, Riew KD: Free hand pedicle screw placement in the thoracic spine: is it safe? **Spine 29:**333–342, 2004
8. Lonstein JE, Denis F, Perra JH, Pinto MR, Smith MD, Winter RB: Complications associated with pedicle screws. **J Bone Joint Surg Am 81:**1519–1528, 1999
9. Merloz P, Tonetti J, Pittet L, Coulomb M, Lavalleé S, Sautot P: Pedicle screw placement using image guided techniques. **Clin Orthop Relat Res 354:**39–48, 1998
10. O'Brien MF, Lenke LG, Mardjetko S, Lowe TG, Kong Y, Eck K, et al: Pedicle morphology in thoracic adolescent idiopathic scoliosis: is pedicle fixation an anatomically viable technique? **Spine 25:**2285–2293, 2000
11. Suk SI, Kim WJ, Lee SM, Kim JH, Chung ER: Thoracic pedicle screw fixation in spinal deformities: are they really safe? **Spine 26:**2049–2057, 2001
12. Suk SI, Lee CK, Kim WJ, Chung YJ, Park YB: Segmental pedicle screw fixation in the treatment of thoracic idiopathic scoliosis. **Spine 20:**1399–1405, 1995
13. Xu R, Ebraheim NA, Ou Y, Yeasting RA: Anatomic considerations of pedicle screw placement in the thoracic spine. Roy-Camille technique versus open-lamina technique. **Spine 23:** 1065–1068, 1998

Manuscript submitted June 8, 2009.
Accepted March 22, 2010.
Address correspondence to: Morio Matsumoto, M.D., Department of Orthopedic Surgery, Keio University School of Medicine, 35 Shinanomachi, Shinjuku, Tokyo #160-8582, Japan. email: kw197251@sc.itc.keio.ac.jp.

THE JOURNAL OF IMMUNOLOGY

Receptor Activator of NF-κB (RANK) Ligand Induces Ectodomain Shedding of RANK in Murine RAW264.7 Macrophages

Akihiro Hakozaki, Masaki Yoda, Takahide Tohmonda, Mitsuru Furukawa, Tomohiro Hikata, Shinichi Uchikawa, Hironari Takaishi, Morio Matsumoto, Kazuhiro Chiba, Keisuke Horiuchi and Yoshiaki Toyama

J Immunol 2010;184;2442-2448; Prepublished online 29 January 2010;
doi:10.4049/jimmunol.0901188
http://www.jimmunol.org/content/184/5/2442

The Journal of Immunology is published twice each month by
The American Association of Immunologists, Inc.,
9650 Rockville Pike, Bethesda, MD 20814-3994.

Print ISSN: 0022-1767 Online ISSN: 1550-6606.

Receptor Activator of NF-κB (RANK) Ligand Induces Ectodomain Shedding of RANK in Murine RAW264.7 Macrophages

Akihiro Hakozaki,* Masaki Yoda,* Takahide Tohmonda,* Mitsuru Furukawa,* Tomohiro Hikata,* Shinichi Uchikawa,* Hironari Takaishi,* Morio Matsumoto,* Kazuhiro Chiba,* Keisuke Horiuchi,*,† and Yoshiaki Toyama*

Osteoclastogenesis is a highly sophisticated process that involves a variety of membrane-bound proteins expressed in osteoblasts and osteoclast precursors. Over the past several years, proteolytic cleavage and release of the ectodomain of membrane-bound proteins, also referred to as ectodomain shedding, has emerged as an important posttranslational regulatory mechanism for modifying the function of cell surface proteins. In line with this notion, several membrane-bound molecules involved in osteoclastogenesis, including CSF-1R and receptor activator of NF-κB ligand (RANKL), are proteolytically cleaved and released from the cell surface. In this study, we investigated whether receptor activator of NF-κB (RANK), one of the most essential molecules in osteoclastogenesis, undergoes ectodomain shedding. The results showed that RANK is released in the form of a soluble monomeric protein and that TNF-α–converting enzyme is involved in this activity. We also identified potential cleavage sites in the juxtamembrane domain of RANK and found that rRANKL induces RANK shedding in a macrophage-like cell line RAW264.7 via TNFR-associated factor 6 and MAPK pathways. Furthermore, we found that RANKL-induced osteoclastogenesis is accelerated in TNF-α–converting enzyme-deficient osteoclast precursors. These observations suggest the potential involvement of ectodomain shedding in the regulation of RANK functions and may provide novel insights into the mechanisms of osteoclastogenesis. ***The Journal of Immunology*****, 2010, 184: 2442–2448.**

Receptor activator of NF-κB (RANK) is one of the most crucial molecules involved in the differentiation, survival, and activation of osteoclasts (1–4). RANK is a type 1 transmembrane protein and is expressed predominantly in immune cells. Association with its cognate ligand, RANK ligand (RANKL), expressed on osteoblasts and stromal cells, is the key event in osteoclast development. As shown in studies on genetically engineered animals, the absence of either of these two molecules or inhibition of the RANKL–RANK association with an endogenous decoy receptor (osteoprotegerin) results in defective osteoclastogenesis in vivo, which is highlighted by the severe loss of osteoclasts and an osteopetrosis-like phenotype (5–7). Because RANKL is also a membrane-bound protein, osteoclast precursors expressing RANK must make cell–cell contact with osteoblasts and stromal cells through the RANK–RANKL association. Thus, the cell surface expression of these two molecules must be tightly regulated to properly sustain osteoclastogenesis during development and adulthood.

In the past decade, a posttranslational mechanism involving the proteolytic cleavage of membrane-bound proteins, also referred to as ectodomain shedding, emerged as a critical processing mechanism for modifying the functions of cell surface proteins (for reviews on ectodomain shedding, see Refs. 8–11). Recent studies showed that the cell surface availability of RANKL in osteoblasts and stromal cells is regulated, at least in part, by ectodomain shedding and that loss of shedding activity in vivo results in a decrease in bone mass due to increased osteoclastogenesis (12–14). Additionally, the cell surface isoform of CSF-1 (also known as M-CSF) and CSF-1R were shown to be proteolytically cleaved to become soluble (15–17). In contrast, it was unknown whether RANK expressed on osteoclasts and their precursors is subjected to ectodomain shedding.

In this study, we show that the extracellular domain of RANK is proteolytically cleaved and released as a soluble monomeric protein. In addition, we identified TNF-α–converting enzyme (TACE) as a crucial enzyme involved in this shedding activity, as well as the sites in the juxtamembrane domain that are required for efficient cleavage. We also found that the shedding activity is upregulated by rRANKL in macrophage-like cell line RAW264.7, indicating that the cell surface availability of RANK is negatively regulated by the association with its ligand. Furthermore, we found that recombinant soluble RANK, which contains the extracellular domain of RANK N terminus to the putative cleavage sites, suppresses RANKL-induced osteoclastogenesis, and that osteoclastogenesis is accelerated in

*Department of Orthopedic Surgery and †Department of Anti-aging Orthopedic Research, School of Medicine, Keio University, Tokyo, Japan

Received for publication April 13, 2009. Accepted for publication December 24, 2009.

This work was supported by Grants-in-Aid for Scientific Research from the Ministry of Education, Culture, Sports, Science, and Technology of Japan (20791051 to A.H. and 21390424 to K.H.), and the Mochida Memorial Foundation, the Takeda Science Foundation, and the Keio University Kanrinmaru project (to K.H.).

Address correspondence and reprint requests to Dr. Keisuke Horiuchi, Department of Orthopedic Surgery, School of Medicine, Keio University, 35 Shinanomachi, Shinjuku-ku, Tokyo 160-8582, Japan. E-mail address: horiuchi@z3.keio.jp

Abbreviations used in this paper: AP, alkaline phosphatase; BMM, bone marrow macrophage; HA, hemagglutinin; mEF, mouse embryonic fibroblast; RANK, receptor activator of NF-κB; $RANK^{AP}$, alkaline phosphatase-tagged RANK expression vector; $RANK^{HA\text{-}Myc}$, HA-epitope and Myc/His-epitope dually tagged receptor activator of NF-κB; RANKL, receptor activator of NF-κB ligand; $sRANK^{HA\text{-}Myc}$, HA-epitope and Myc/His-epitope dually tagged soluble receptor activator of NF-κB; SS, signaling sequence; TACE, TNF-α–converting enzyme; TM, transmembrane domain; TRAF6, TNFR-associated factor 6; TRAP, tartrate-acid resistant alkaline phosphatase; Wt, wild-type.

www.jimmunol.org/cgi/doi/10.4049/jimmunol.0901188

osteoclast precursors lacking TACE. These observations reveal a previously unknown contribution of ectodomain shedding to the functions of RANK and may provide novel insights into the mechanisms involved in osteoclastogenesis.

Materials and Methods

Cell lines and reagents

TACE-deficient and wild-type mouse embryonic fibroblasts (mEFs) derived from E13.5 embryos were immortalized, as previously described (18, 19). RAW264.7 cells and COS-7 cells were obtained from the RIKEN cell bank. The anti-hemagglutinin (HA) mAbs were from Sigma-Aldrich (HA-7; St. Louis, MO) and Roche Diagnostics (3F10; Indianapolis, IN). Anti-Myc polyclonal Ab was purchased from Medical and Biological Laboratories (Nagoya, Japan). Anti-Myc mAbs were from Abgent (9E10; San Diego, CA) and Medical and Biological Laboratories (PL-14). TNFR-associated factor 6 (TRAF6) inhibitory peptide was from Imgenex (San Diego, CA). The fluorochrome-conjugated Abs and streptavidin used in immunostaining were purchased from Jackson ImmunoResearch Laboratories (West Grove, PA). Anti-human placental alkaline phosphatase Ab was from Sigma-Aldrich (8B6). U0126, SP600125, SB202190, and GM6001 were from Calbiochem (San Diego, CA). All other reagents were obtained from Sigma-Aldrich, unless otherwise indicated.

Generation of RANK expression vectors

A cloning vector containing murine RANK cDNA was generously provided by Dr. Akira Kudo (Tokyo Institute of Technology) and was used as a PCR template to generate epitope-tagged RANK expression vectors. HA-epitope and Myc/His-epitope dually tagged RANK ($RANK^{HA\text{-}Myc}$) was generated by inserting an HA-epitope sequence after the signal peptide sequence of the RANK cDNA and by cloning it into the pcDNA4/Myc-His expression vector (Invitrogen, Carlsbad, CA). Alkaline phosphatase (AP)-tagged RANK expression vector ($RANK^{AP}$) was generated by cloning RANK cDNA (Lys^{171}-Ala^{242}) into pAPtag5 (Genhunter, Nashville, TN) (see Fig. 1*A* for the schema of the constructs). Cell-expression of $RANK^{HA\text{-}Myc}$ and $RANK^{AP}$ was confirmed by Western blot and immunostaining (Fig. 1*B* and data not shown). $RANK^{AP}$ vector was further used as a PCR template to generate cleavage-site mutant RANK expression vectors (Fig. 5*B*). Mutations in the juxtamembrane region of RANK were introduced by a PCR-based method using a KOD plus Mutagenesis kit (Toyobo, Tokyo, Japan), according to the manufacturer's instructions.

Cell culture, transfection, and shedding assay

COS-7 cells and mEFs were grown in DMEM supplemented with 5% FCS and antibiotics. RAW264.7 cells were grown in α-MEM supplemented with 10% FCS and antibiotics. Bone marrow cells collected from the tibiae and femurs of 6–10-wk-old $Tace^{flox/flox}$/*LysM-Cre*$^{+}$ mice (*Tace/LysM* mice) (19) or littermate control mice were grown in α-MEM with 10% FCS, antibiotics, and 30 ng/ml recombinant mouse M-CSF-1 (WAKO, Osaka, Japan) for 3 d, and then used as bone marrow macrophages (BMMs). The cells were transfected with the expression vectors by using FuGENE HD (Roche Diagnostics), according to the manufacturer's instructions. Fresh Opti-MEM (Invitrogen) medium, with or without PMA and/or GM6001, was added 18–24 h after transfection, and the cells were incubated for 1 h. The supernatants were collected and cleared by centrifugation to remove cell debris. The activity of AP in the supernatant, which reflects the amount of AP-tagged RANK released from the cell surface, was measured by colorimetry, as described previously (15, 20). The supernatant from nontransfected cells incubated with the substrate for the same amount of time was used as a spectrophotometric blank to offset background AP activity. In-gel visualization of AP activity in the supernatant was also performed, as previously described (20). The cleared samples were concentrated using ConA-Sepharose lectin beads (GE Healthcare Bio-Sciences, Piscataway, NJ) and separated by 10% SDS-PAGE. The AP activity in the gel was visualized with NBT/5-bromo-4-chloro-3-indolyl phosphate (Sigma-Aldrich). All experiments were repeated at least three times in duplicate with similar results.

Identification of the cleavage sites for TACE in peptides corresponding to the juxtamembrane domain of RANK

Peptide cleavage assays were performed, as previously described (21). In brief, a peptide corresponding to the juxtamembrane region of RANK (SDVVCSSSMTLRRPPKEAQAY) was incubated with rTACE (R&D Systems, Minneapolis, MN) for 4–8 h at 37°C, and the cleavage products were analyzed by liquid chromatography MALDI time-off light mass spectrometry (BIFLEX3, Bruker, Billerica, MA).

Immunoprecipitation and Western blot analysis

Cells were lysed with 1% Triton-X 100/PBS containing a protease inhibitor mixture and 10 mM 1,10-phenanthroline (Sigma-Aldrich). The lysates were cleared by centrifugation and incubated with anti-Myc polyclonal Ab for 12 h, and then with protein G-coupled Sepharose beads for 1 h at 4°C with rotary agitation. After separating the lysates by 10% SDS-PAGE, Western blot analysis was performed using anti-HA and anti-Myc mAbs.

Flow cytometry analysis

COS-7 cells transiently expressing $RANK^{HA\text{-}Myc}$ were incubated at 37°C for 1 h with growth medium in the presence or absence of PMA and/or GM6001. The cells were washed twice with ice-cold PBS, trypsinized, and resuspended in ice-cold 5% BSA/PBS. Subsequently, the cells were incubated with anti-HA Ab at 4°C for 30 min and then washed with ice-cold 5% BSA/PBS. The Abs on the cell surface were detected with a fluorochrome-conjugated secondary Ab. RAW264.7 cells and BMMs were incubated with Opti-MEM containing PMA and/or GM6001 at 37°C for 1 h. The cells were collected using cell dissociation solution (Sigma-Aldrich) and incubated with ice-cold BSA/PBS containing 2 mM EDTA and anti-mouse CD16/32 Ab (clone, 93; BioLegend, San Diego, CA) for 15 min to block nonspecific binding of IgG to the Fc receptor. RAW264.7 cells were further incubated with biotin-labeled anti-mouse RANK Ab (R12-31, BioLegend), and BMMs were incubated with anti-mouse RANK Ab and anti-CD11b Ab (M1/70, BioLegend). The biotin-labeled anti-mouse RANK Ab was detected by allophycocyanin-streptavidin (BioLegend). Biotin-labeled rat IgG2aκ was used as an isotype control. Fluorochrome-labeled cells were analyzed by a laser flow cytometer (FACSCalibur system, BD Biosciences, San Jose, CA) and by FlowJo software (Tree Star, Ashland, OR).

Generation of recombinant soluble RANK

HA-epitope and Myc/His-epitope dually tagged soluble RANK ($sRANK^{HA\text{-}Myc}$) expression vector was generated by cloning $RANK^{HA\text{-}Myc}$ cDNA (Met^{1}-Ser^{198}) into pcDNA4.0 (Fig.7*A*, *left panel*). The construct was introduced into COS-7 cells by using FuGENE HD, and the cells were cultured for 2 d. At the end of the incubation, the cells were lysed in lysis buffer, and $sRANK^{HA\text{-}Myc}$ in the lysates was collected using a c-Myc-tagged protein purification kit (Medical and Biological Laboratories), as instructed by the manufacturer. Expression of $sRANK^{HA\text{-}Myc}$ in COS-7 cells was confirmed by Western blot (Fig. 7*A*, *right panel*).

Osteoclastogenesis assay

BMMs were plated on 48-well plates at 1×10^5 cells/well and incubated with 30 ng/ml CSF-1 and 50 ng/ml rRANKL in the presence or absence of $sRANK^{HA\text{-}Myc}$ (~50 ng/ml) for 5 d. The cells were stained for tartrate-resistant acid phosphatase (TRAP), and the number of osteoclasts (defined as TRAP-positive multinucleated cells with more than three nuclei) was counted under the microscope.

Real-time RT-PCR assay

Total RNA was extracted using an RNeasy Mini Kit (Qiagen, Valencia, CA) and was reverse-transcribed by ReverTra ACE (Toyobo). PCR amplification and quantification were done using SYBR Premix ExTaq II (Takara Shuzo, Otsu, Japan) and the LightCycler Quick System (Roche Diagnostics). Relative mRNA expression levels were obtained by normalizing to β-actin expression. Results are representative of at least three individual experiments.

Statistical analysis

The Student *t* test for two samples, assuming equal variances, was used to calculate the *p* values. The *p* values <0.05 were considered statistically significant. All data are presented as mean ± SD.

Results

The extracellular domain of RANK can be cleaved to become a soluble protein

We first investigated whether RANK could be proteolytically cleaved and released into the supernatant by conducting cell-based assays. To facilitate the detection of cleaved RANK, we generated an HA-epitope (inserted between the signaling sequence and extracellular domain) and Myc/6×His (added to the C terminus of the intracellular domain) dually tagged RANK construct (Fig. 1*A*) and introduced it into COS-7 cells. As shown in Fig. 1*B*, an ~85-kDa protein was detected in the lysate from $RANK^{HA\text{-}Myc}$-transfected

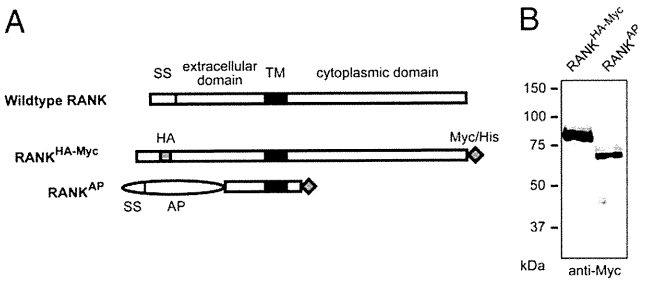

FIGURE 1. *A*, Schema of HA- and Myc/His-tagged RANK ($RANK^{HA\text{-}Myc}$) and AP-tagged RANK ($RANK^{AP}$) constructs. SS, signaling sequence; TM, transmembrane domain. *B*, Western blot analysis of $RANK^{HA\text{-}Myc}$ and $RANK^{AP}$ expressed in COS-7 cells.

COS-7 cells. Cell surface expression of the $RANK^{HA\text{-}Myc}$ protein introduced into COS-7 cells was confirmed by immunostaining (data not shown). We next examined the supernatant from $RANK^{HA\text{-}Myc}$-transfected COS-7 cells for the presence of cleaved soluble RANK. The supernatants were concentrated with ConA-Sepharose lectin beads and subjected to Western blot analysis with anti-HA Ab, which recognizes the extracellular domain of $RANK^{HA\text{-}Myc}$. Under unchallenged conditions, almost no protein was found, but an ~25-kDa band was detected in the supernatant from the cells stimulated with PMA (Fig. 2*A*). Moreover, the intensity of the band was suppressed by the addition of a broad metalloprotease inhibitor, GM6001, indicating that the proteolytic activity is metalloprotease dependent. Accordingly, when the cell surface expression level of $RANK^{HA\text{-}Myc}$ in COS-7 cells was investigated by flow cytometry, a significant decrease was observed in the cells treated with PMA, whereas treatment with GM6001 abolished the effects of PMA stimulation (Fig. 2*B*). To confirm these observations, we attempted to determine whether the cleaved stub of $RANK^{HA\text{-}Myc}$ remaining in the cells could be detected in the cell lysates. The lysates from the cells incubated with or without PMA were immunoprecipitated with rabbit anti-Myc sera and probed with murine anti-HA Ab and then with murine anti-Myc Ab. As expected, full-length RANK was found when the sample was analyzed with anti-HA Ab, whereas when the membrane was washed and reprobed with anti-Myc Ab, which recognizes the cytoplasmic end of $RANK^{HA\text{-}Myc}$, an ~60-kDa band, in addition to the full-length RANK, was obtained (Fig. 2*C*). Identical results were obtained with a murine anti-Myc Ab from a different clone (data not shown). Taken together, these observations suggest that $RANK^{HA\text{-}Myc}$ that has been transfected into COS-7 cells can be proteolytically processed and released into the supernatant and that the PMA-stimulated proteolytic activity is metalloprotease dependent.

Cleaved soluble RANK is present in the form of a monomer protein

It was shown that RANK forms a trimer without ligand binding and that the self-association of RANK is mediated through its cytoplasmic tail (22). Based on these observations, we hypothesized that, upon cleavage, the extracellular domain of RANK is released in the supernatant as a monomer protein. To test this hypothesis, we analyzed the cell lysates and supernatants of COS-7 cells transfected with $RANK^{HA\text{-}Myc}$ by Western blot with or without the addition of a reducing agent, DTT. Under nonreducing conditions (without the addition of DTT), as much as half of the $RANK^{HA\text{-}Myc}$ in the cell lysate appeared in the form of a >200-kDa protein, presumably representing a RANK trimer, whereas, under reducing conditions, the >200-kDa band disappeared, and only the 85-kDa band was detected (Fig. 3*A*). In contrast, the protein species detected in the supernatant were insensitive to DTT and seemed to be identical under nonreducing and reducing conditions (Fig. 3*B*). These results suggest that RANK cannot form a trimer after it is released from the cell surface and that the cleaved extracellular domain is present in the supernatant in the form of a monomer.

TACE mediates cleavage of RANK

Because the combination of a response to short-term PMA stimulation and the sensitivity to metalloprotease inhibitors is a hallmark of TACE activity (23), we next attempted to determine whether TACE was involved in the ectodomain shedding of RANK. To facilitate the transfection and the detection of cleaved RANK in the supernatant, we used the AP reporter system (20) and generated a truncated RANK construct with an AP module added to its N terminus ($RANK^{AP}$, Fig. 1*A*). We first investigated whether this construct could reproduce the shedding properties of $RANK^{HA\text{-}Myc}$ by introducing $RANK^{AP}$ into wild-type mEFs and measuring AP activity in the lysates and supernatants by in-gel staining, as

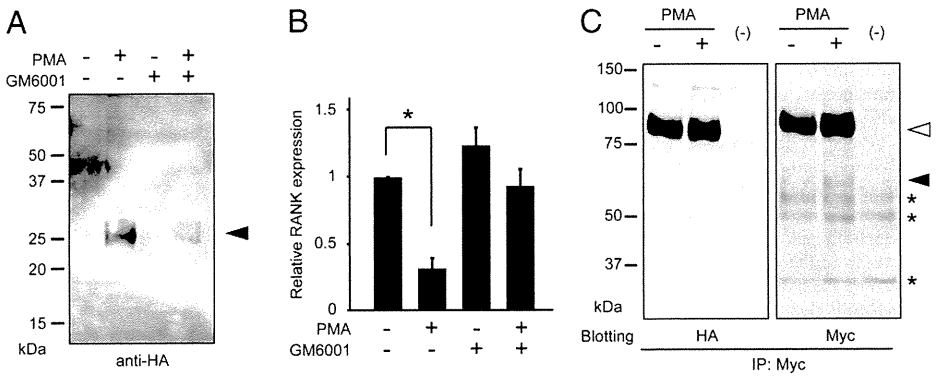

FIGURE 2. Cleavage of RANK in COS-7 cells. *A*, The extracellular domain of $RANK^{HA\text{-}Myc}$ is cleaved and released into the supernatant. COS-7 cells transfected with $RANK^{HA\text{-}Myc}$ were incubated with PMA (25 ng/ml) and/or GM6001 (10 μM) for 1 h. Supernatants were concentrated and analyzed by Western blot with anti-HA Ab. A protein weighing ~25 kDa was detected in PMA-treated cells (arrowhead). *B*, The same cells as in *A* were treated with PMA and/or GM6001 and then incubated with anti-HA Ab. The bound Abs were detected with fluorochrome conjugated secondary Ab and evaluated by flow cytometry. The means of the values obtained in three independent experiments are shown. $*p < 0.05$. *C*, Membrane-bound stubs of RANK were detected in $RANK^{HA\text{-}Myc}$-transfected COS-7 cells. COS-7 cells transiently expressing $RANK^{HA\text{-}Myc}$ were stimulated with PMA, and cell lysates were immunoprecipitated with anti-Myc Ab. The immunoprecipitates were blotted with anti-HA Ab (which recognizes the extracellular domain of $RANK^{HA\text{-}Myc}$) and anti-Myc Ab (which recognizes the cytoplasmic domain of $RANK^{HA\text{-}Myc}$). White arrowhead, full-length $RANK^{HA\text{-}Myc}$; black arrowhead, membrane-bound stub; *, nonspecific bands; (−), nontransfected COS-7 cells.

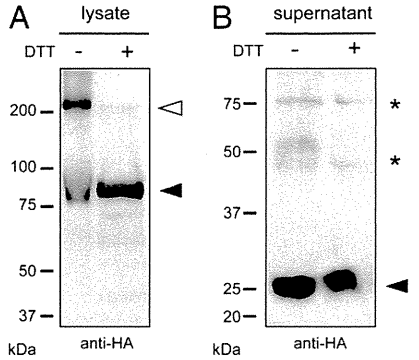

FIGURE 3. Cleaved RANK is released as a monomeric protein. The lysates (*A*) and supernatants (*B*) from $RANK^{HA\text{-}Myc}$-transfected COS-7 cells were analyzed by Western blot under nonreducing [DTT(−)] or reducing [DTT(+)] conditions. White arrowhead, trimer; black arrowheads, monomer; *, nonspecific bands.

described in *Materials and Methods*. We obtained results similar to those observed with $RANK^{HA\text{-}Myc}$, indicating that $RANK^{AP}$ has shedding properties similar to those of $RANK^{HA\text{-}Myc}$ (Fig. 4*A*); therefore, we used this construct for the subsequent studies. To investigate the possible involvement of TACE in the processing of RANK, we next used immortalized mEFs derived from *Tace*$^{-/-}$ embryos (19). As shown in Fig. 4*B*, the PMA-stimulated activity was completely abolished in *Tace*$^{-/-}$ mEFs, and reintroduction of TACE fully restored it. Furthermore, we evaluated the cell surface expression of endogenous RANK in BMMs derived from wild-type mice and the mutant mice in which TACE is inactivated in monocytes/macrophages [*Tace/LysM* mice (19)] by flow cytometry. In wild-type BMMs, there was a significant decrease in the RANK expression levels after PMA treatment, whereas in BMMs derived from *Tace/LysM* mice the majority of the cell population was unaffected by PMA stimulation and maintained the RANK expression at a comparable level to the cells that were not treated with PMA (Fig. 4*C*). Taken together, these observations indicate that TACE is primarily responsible for the PMA-stimulated cleavage of RANK in osteoclast precursors.

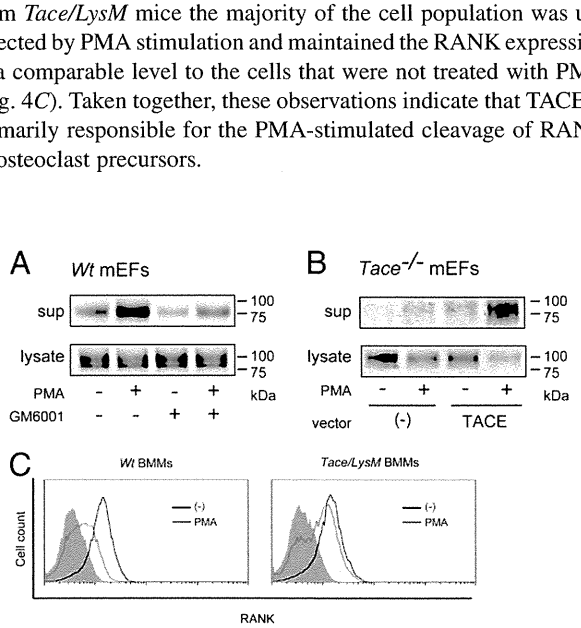

FIGURE 4. TACE mediates RANK shedding. *A*, $RANK^{AP}$-transfected wild-type (Wt) mEFs were incubated with PMA and/or GM6001 for 1 h. The supernatants and lysates were analyzed for AP activity by in-gel staining, as described in *Materials and Methods*. *B*, *Tace*$^{-/-}$ mEFs were transfected with $RANK^{AP}$ and an empty vector (−) or TACE expression vector. The supernatants and lysates of cells that had been stimulated or not with PMA were analyzed for AP activity by in-gel staining. *C*, BMMs derived from wild-type (Wt) mice or *Tace/LysM* mice were incubated with or without PMA, and the cell surface expression levels of RANK were analyzed by flow cytometry. The shaded areas represent isotype Ab.

RANK is cleaved in the stalk region

To identify the potential RANK cleavage site(s) in more detail and determine whether TACE directly cleaves RANK, we synthesized a peptide covering the juxtamembrane domain of RANK (Ser^{191}-Tyr^{211}) and incubated it with rTACE. Based on the results of the mass spectrometry analysis, we concluded that rTACE directly cleaved the peptide and deduced two potential cleavage sites in the juxtamembrane domain of RANK: a major site between Thr^{200}-Leu^{201} and a minor site between Met^{199}-Thr^{200} (Fig. 5*A* and data not shown). We next generated several mutant $RANK^{AP}$ constructs (Fig. 5*A*, Mut1–6) and investigated how the mutations in the putative cleavage sites affected the cleavage efficiency. Cell surface expression of the mutants (Mut1–6) was confirmed by immunostaining and confocal microscopic analysis (data not shown). As shown in Fig. 5*B*, when Met^{199}-Thr^{200}-Leu^{201} was replaced with Ile-Ser-Pro (Mut1) or with Ile-Thr-Pro (Mut5), there was a significant decrease in the AP activity in the supernatant. Although cleavage of these mutants was still increased by PMA stimulation, overall shedding efficiency was significantly diminished. In contrast, the shedding efficiency of Mut2–4 was comparable to that of the wild-type control. The deletion mutant (Mut6), in which Met^{199}-Thr^{200}-Leu^{201} had been removed, was as resistant to shedding as Mut1 and Mut5. Taken together, these observations suggest that, although RANK shedding by TACE is not absolutely dependent on the Met^{199}-Thr^{200}-Leu^{201} sequence in the juxtamembrane domain, it is required for efficient cleavage.

RANK shedding in RAW264.7 cells is upregulated by rRANKL

To extend our findings, we next investigated whether RANK is cleaved in a macrophage-like cell line (RAW264.7) that expresses endogenous RANK and differentiates into multinucleated osteoclasts in response to RANKL stimulation. Expression of TACE in this cell line was confirmed by Western blot (data not shown). RAW264.7 cells transfected with $RANK^{AP}$ were incubated with PMA and/or GM6001, and the supernatant was analyzed for AP activity by colorimetry, as described in *Materials and Methods*. As

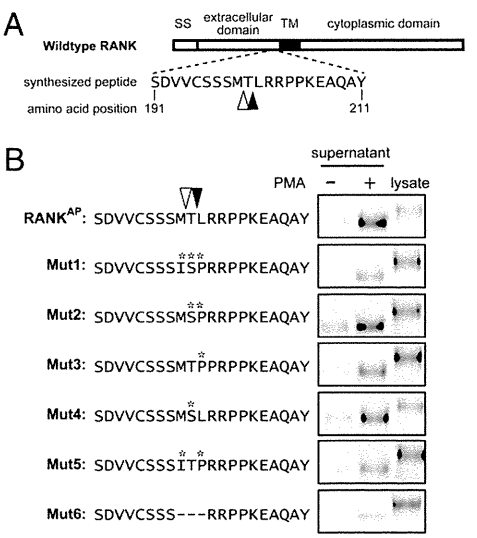

FIGURE 5. *A*, Schema of the synthesized peptide used in the peptide-cleavage assay and the putative cleavage sites (major site, black arrowhead; minor site, white arrowhead) deduced from the results of the mass spectrometry analysis of the cleaved peptides. *B*, Evaluation of the shedding efficiency of $RANK^{AP}$ mutants (Mut1–6). The mutant constructs were introduced into COS-7 cells, and the AP activity in the supernatants and lysates was visualized by in-gel staining. Asterisks indicate substituted amino acids.

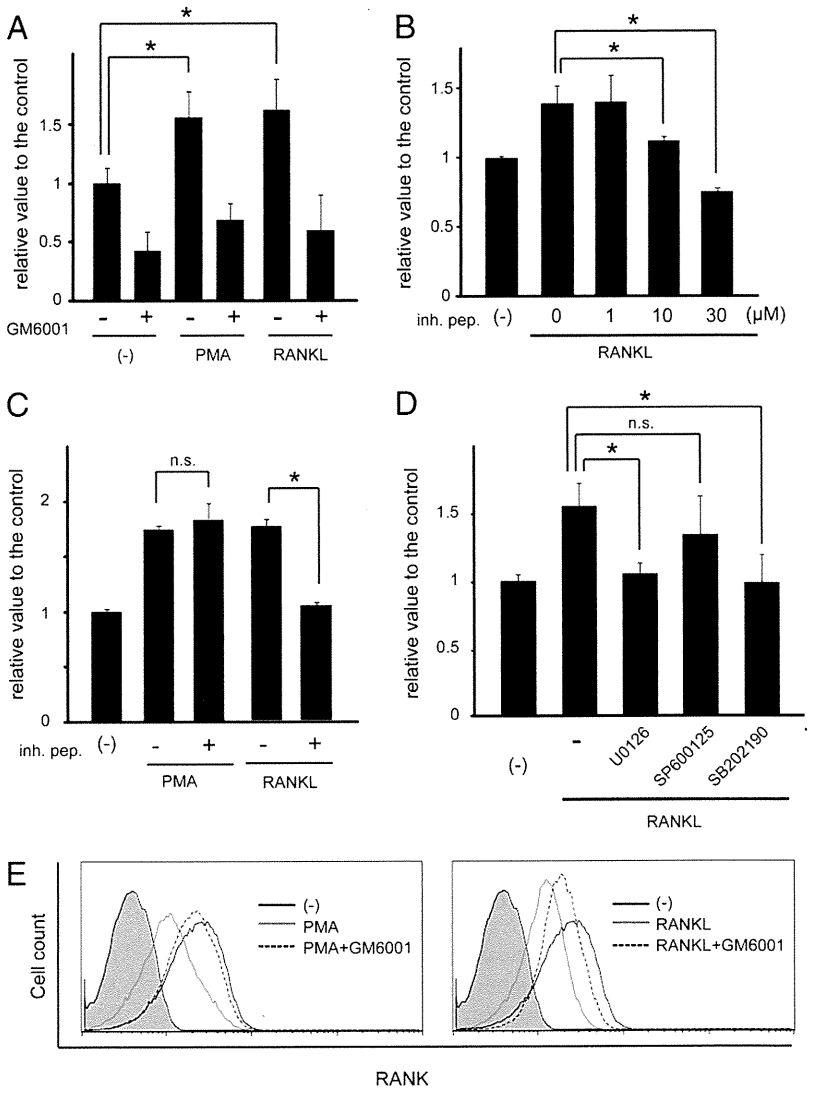

FIGURE 6. RANKL upregulates RANK shedding in RAW264.7 cells. *A*, $RANK^{AP}$-transfected RAW264.7 cells were incubated with PMA (25 ng/ml) or soluble RANKL (100 ng/ml) for 1 h, and AP activity released into the supernatant was analyzed by colorimetry. *B*, TRAF6 inhibitory peptide inhibited RANKL-induced shedding activity. $RANK^{AP}$-transfected RAW264.7 cells were incubated with soluble RANKL (100 ng/ml) in the presence of the inhibitory peptide (inh. pep., 0–30 μM). *C*, TRAF6 inhibitory peptide (30 μM) abolished RANKL-induced shedding activity but had little effect on PMA-stimulated RANK shedding. *D*, Evaluation of the effects of the MAPK inhibitors U0126 (5 μM), SB202190 (20 μM), and SP600125 (20 μM) on the RANKL-induced RANK shedding activity. $*p < 0.05$. *E*, RAW264.7 cells were incubated with PMA (10 nM, *left panel*) or RANKL (100 ng/ml, *right panel*) in the presence or absence of GM6001 (25 μM), and the cell surface expression levels of RANK were analyzed by flow cytometry. The shaded areas represent isotype Ab.

shown in Fig. 6*A*, the results were comparable to those observed in wild-type mEFs (Fig. 4*A*), indicating that RANK is similarly processed in RAW264.7 cells. Based on an analogy to the induction of the shedding of vascular endothelial growth factor receptor by its ligand, vascular endothelial growth factor-A (24), we next investigated whether RANKL could trigger the cleavage of RANK. As shown in Fig. 6*A*, RANK shedding was upregulated by rRANKL in RAW264.7 cells to a level comparable to that induced by PMA, and the increased activity was abolished by the addition of GM6001. It has been well established that following ligand binding, RANK activates various signaling pathways essential for osteoclast development and that the initial step in the signaling involves binding of TRAF6 to the cytoplasmic domain of RANK. To explore whether RANKL-induced RANK shedding was TRAF6 dependent, we used a TRAF6 inhibitory peptide, which functions as a TRAF6 decoy by binding to the TRAF6-binding motif of RANK (25), and examined how it would affect RANKL-induced RANK shedding activity. When $RANK^{AP}$-transfected RAW264.7 cells were incubated in the presence of TRAF6 inhibitory peptide, it had a dose-dependent inhibitory effect on RANKL-induced shedding activity (Fig. 6*B*). The inhibitory effect was specific to TRAF6, because PMA-induced shedding activity, which does not involve TRAF6 activation, was insensitive to the inhibitory peptide at a concentration at which RANKL-induced shedding was completely abolished (Fig. 6*C*). We also found that RANKL-induced shedding was sensitive to U0126 (MEK inhibitor) and SB202190 (p38 inhibitor) but not to SP600125 (JNK inhibitor), indicating that RANKL-induced shedding activity is TRAF6 and MAPK dependent (Fig. 6*D*). To further confirm the observation that RANK shedding can be induced by RANKL stimulation, we examined the cell surface expression of endogenous RANK by flow cytometry. As shown in Fig. 6*E*, incubation with PMA or RANKL significantly decreased the cell surface expression of RANK in RAW264.7 cells, and this activity was abolished by the addition of GM6001.

RANK shedding functions as a negative regulator in RANKL-induced osteoclastogenesis in vitro

To gain insight on the physiological relevance of RANK shedding, we generated recombinant soluble RANK composed of the extracellular region of RANK N terminus to the putative cleavage site (Met^{1}-Ser^{198}, Fig. 7*A*), and examined how the cleaved extracellular domain of RANK would affect RANKL-induced osteoclastogenesis in vitro. RAW264.7 cells were incubated with rRANKL in the presence or absence of $sRANK^{HA\text{-}Myc}$ for 5 d, and the number of TRAP-positive multinucleated cells was evaluated. As shown in Fig. 7*B*, the addition of $sRANK^{HA\text{-}Myc}$ almost completely abolished RANKL-induced osteoclastogenesis, indicating that cleaved soluble RANK functions as an antagonist to RANKL in a similar manner to osteoprotegerin, an endogenous decoy receptor for RANKL.

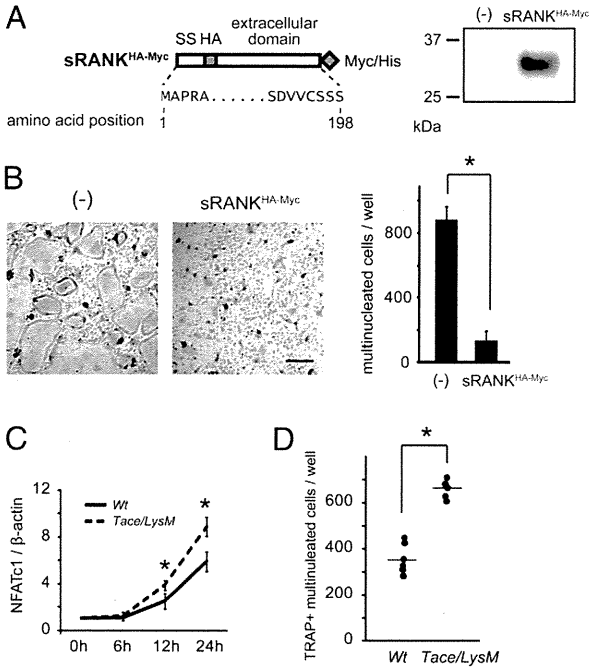

FIGURE 7. RANK shedding serves as a negative regulator for osteoclastogenesis. *A*, Schematic representation of the sRANK^{HA-Myc} construct (*left panel*). The supernatant from sRANK^{HA-Myc}-transfected COS-7 cells were concentrated, and the sRANK^{HA-Myc} was detected by Western blot using anti-Myc Ab (*right panel*). *B*, RAW264.7 cells were incubated with RANKL (50 ng/ml) in the absence (−) or presence of sRANK^{HA-Myc}. The number of TRAP-positive multinucleated cells was counted on day 5. Scale bar, 250 μm; original magnification ×40. BMMs derived from wild-type (Wt) mice or *Tace/LysM* mice were incubated with RANKL and CSF-1 as described in *Materials and Methods*. The expression levels of NFATc1 and β-actin were evaluated at the designated time points (*C*), and the number of TRAP-positive multinucleated cells was counted on day 4 (*D*). $*p < 0.05$.

Furthermore, we found that TACE-deficient BMMs derived from *Tace/LysM* mice exhibited increased levels of NFATc1, a transcription factor essential for osteoclastogenesis, after RANKL stimulation (Fig. 7*C*) and that RANKL-induced osteoclastogenesis is accelerated compared with the wild-type control (Fig. 7*D*). These observations indicate that RANK shedding functions as a negative regulator for osteoclastogenesis, presumably via the production of soluble RANK and by decreasing cell surface RANK availability in osteoclast precursors.

Discussion

Several membrane-bound molecules involved in osteoclast development, including RANKL (12), CSF-1R (16), TNF-α (26), and the membrane-bound isoform of CSF-1 (15), are proteolytically cleaved to become soluble. The current study shows for the first time that RANK, a molecule essential for osteoclastogenesis, also undergoes ectodomain shedding and is released as a monomeric protein. We also found by means of cell-based assays, using TACE-deficient cells, that TACE is involved in RANK shedding activity and that this activity can be upregulated by RANKL in macrophage-like cell line RAW264.7. These results indicate a potential involvement of ectodomain shedding of RANK in the regulation of osteoclastogenesis.

Consistent with the results of a previous study (22), RANK^{HA-Myc} introduced into COS-7 cells self-assembled in the absence of RANKL (Fig. 3*A*), whereas the cleaved extracellular domain of RANK released in the supernatant was in the form of a monomeric protein, not as a trimer, indicating that the cytoplasmic domain or juxtamembrane domain is required for the self-association of RANK and that once cleaved from the cell surface, RANK is no longer able to form a trimer. In contrast, it is possible that RANK is resistant to ectodomain shedding when it is in the trimetric conformation and that only the unassociated monomer proteins are cleaved from the cell surface.

The consequences of ectodomain shedding of receptors can be complex in some cases. Ectodomain shedding of receptors can result in downregulation of receptor availability on the cell surface and can simultaneously give rise to soluble receptors, which have a potential to function as decoy receptors and to interfere with ligand–receptor association. Moreover, as in the case of CD44 and Notch (27–29), ectodomain shedding of receptors may be necessary to trigger intramembranous cleavage by presenilin and the release of the cytoplasmic domain into the cytoplasm. For example, it is well established that cleaved TNFR1 and TNFR2 are capable of binding to TNF-α and suppressing TNF-α–TNFR signaling and that dysregulation of the shedding of these receptors results in aberrant immunoreactions (30–32). Similarly, recombinant soluble RANK (Glu^{30}-Pro^{213}) and RANK-Fc were demonstrated to inhibit RANKL-induced osteoclastogenesis in vitro and to prevent the formation of metastatic bone lesions in xenograft tumor models (33–36). We also generated soluble RANK composed of the extracellular domain N terminus to the putative cleavage sites and observed a similar inhibitory effect on RANKL-induced osteoclastogenesis in vitro. These observations suggest that the cleaved extracellular domain of RANK is biologically active and potentially functions as a decoy receptor that blocks RANKL binding in a manner similar to that of osteoprotegerin. Because osteoprotegerin can bind not only to RANKL but also to the TNF-related apoptosis-inducing ligand (TRAIL/Apo2 ligand) (37), soluble RANK may function as a more specific inhibitor of RANKL.

Based on the observations that cell surface expression of RANK decreases following RANKL stimulation, it is tempting to hypothesize a negative feedback loop in which RANKL induces RANK shedding and, thereby, downregulates RANKL–RANK signaling during osteoclast development. In accordance, we found that TACE-deficient BMMs form multinucleated cells more rapidly than did the control BMMs and that the expression of NFATc1 is upregulated in TACE-deficient BMMs, indicating that RANK shedding negatively regulates osteoclastogenesis. However, in contrast, no overt bone defects were found in *Tace/LysM* mice, in which TACE is inactivated in monocytes and macrophages (19), at least under unchallenged conditions (data not shown). Thus, other enzyme(s) may compensate for the lack of TACE in the cleavage of RANK, or the regulation of cell surface RANK availability may also be regulated by different mechanisms that do not involve ectodomain shedding (e.g., via endocytosis). Furthermore, it is also possible that the lack of TACE leads to an increase in the amount of other cell surface proteins, which may function in an antiosteoclastogenic manner, and offsets the effects of enhanced RANK signaling. Further research, including a generation of uncleavable mutant RANK knock-in mice, is needed to elucidate the significance of RANK shedding and its impact on osteoclastogenesis.

In conclusion, the current study demonstrated that RANK is subjected to ectodomain shedding by TACE and identified potential cleavage sites in the juxtamembrane domain of RANK. The cleavage of RANK should decrease its availability on osteoclasts and their precursors and simultaneously generate soluble decoy receptors that may inhibit the RANKL–RANK association. Moreover, the observation that RANKL–RANK signaling induces RANK shedding suggests a possible negative-feedback mechanism regulating the cell surface availability of RANK on osteoclasts and their precursors. Therefore, upregulation of RANK shedding via TACE

activation may be beneficial in suppressing overt osteoclastogenesis under pathological conditions, including rheumatoid arthritis, bone metastasis, and osteoporosis.

Acknowledgments

We thank Dr. Akira Kudo for murine RANK cDNA and Shizue Tomita for excellent technical assistance.

Disclosures

The authors have no financial conflicts of interest.

References

1. Theoleyre, S., Y. Wittrant, S. K. Tat, Y. Fortun, F. Redini, and D. Heymann. 2004. The molecular triad OPG/RANK/RANKL: involvement in the orchestration of pathophysiological bone remodeling. *Cytokine Growth Factor Rev.* 15: 457–475.
2. Boyle, W. J., W. S. Simonet, and D. L. Lacey. 2003. Osteoclast differentiation and activation. *Nature* 423: 337–342.
3. Asagiri, M., and H. Takayanagi. 2007. The molecular understanding of osteoclast differentiation. *Bone* 40: 251–264.
4. Wada, T., T. Nakashima, N. Hiroshi, and J. M. Penninger. 2006. RANKL-RANK signaling in osteoclastogenesis and bone disease. *Trends Mol. Med.* 12: 17–25.
5. Simonet, W. S., D. L. Lacey, C. R. Dunstan, M. Kelley, M. S. Chang, R. Lüthy, H. Q. Nguyen, S. Wooden, L. Bennett, T. Boone, et al. 1997. Osteoprotegerin: a novel secreted protein involved in the regulation of bone density. *Cell* 89: 309–319.
6. Kong, Y. Y., H. Yoshida, I. Sarosi, H. L. Tan, E. Timms, C. Capparelli, S. Morony, A. J. Oliveira-dos-Santos, G. Van, A. Itie, et al. 1999. OPGL is a key regulator of osteoclastogenesis, lymphocyte development and lymph-node organogenesis. *Nature* 397: 315–323.
7. Dougall, W. C., M. Glaccum, K. Charrier, K. Rohrbach, K. Brasel, T. De Smedt, E. Daro, J. Smith, M. E. Tometsko, C. R. Maliszewski, et al. 1999. RANK is essential for osteoclast and lymph node development. *Genes Dev.* 13: 2412–2424.
8. Murphy, G., A. Murthy, and R. Khokha. 2008. Clipping, shedding and RIPping keep immunity on cue. *Trends Immunol.* 29: 75–82.
9. Kheradmand, F., and Z. Werb. 2002. Shedding light on sheddases: role in growth and development. *Bioessays* 24: 8–12.
10. Overall, C. M., and C. P. Blobel. 2007. In search of partners: linking extracellular proteases to substrates. *Nat. Rev. Mol. Cell Biol.* 8: 245–257.
11. Blobel, C. P. 2000. Remarkable roles of proteolysis on and beyond the cell surface. *Curr. Opin. Cell Biol.* 12: 606–612.
12. Hikita, A., I. Yana, H. Wakeyama, M. Nakamura, Y. Kadono, Y. Oshima, K. Nakamura, M. Seiki, and S. Tanaka. 2006. Negative regulation of osteoclastogenesis by ectodomain shedding of receptor activator of NF-kappaB ligand. *J. Biol. Chem.* 281: 36846–36855.
13. Lum, L., B. R. Wong, R. Josien, J. D. Becherer, H. Erdjument-Bromage, J. Schlöndorff, P. Tempst, Y. Choi, and C. P. Blobel. 1999. Evidence for a role of a tumor necrosis factor-α (TNF-α)-converting enzyme-like protease in shedding of TRANCE, a TNF family member involved in osteoclastogenesis and dendritic cell survival. *J. Biol. Chem.* 274: 13613–13618.
14. Hikita, A., Y. Kadono, H. Chikuda, A. Fukuda, H. Wakeyama, H. Yasuda, K. Nakamura, H. Oda, T. Miyazaki, and S. Tanaka. 2005. Identification of an alternatively spliced variant of Ca2+-promoted Ras inactivator as a possible regulator of RANKL shedding. *J. Biol. Chem.* 280: 41700–41706.
15. Horiuchi, K., T. Miyamoto, H. Takaishi, A. Hakozaki, N. Kosaki, Y. Miyauchi, M. Furukawa, J. Takito, H. Kaneko, K. Matsuzaki, et al. 2007. Cell surface colony-stimulating factor 1 can be cleaved by TNF-α converting enzyme or endocytosed in a clathrin-dependent manner. *J. Immunol.* 179: 6715–6724.
16. Rovida, E., A. Paccagnini, M. Del Rosso, J. Peschon, and P. Dello Sbarba. 2001. TNF-α-converting enzyme cleaves the macrophage colony-stimulating factor receptor in macrophages undergoing activation. *J. Immunol.* 166: 1583–1589.
17. Horiuchi, K., and Y. Toyama. 2008. Posttranslational regulation of cell-surface colony-stimulating factor-1. *Crit. Rev. Immunol.* 28: 215–227.
18. Weskamp, G., H. Cai, T. A. Brodie, S. Higashyama, K. Manova, T. Ludwig, and C. P. Blobel. 2002. Mice lacking the metalloprotease-disintegrin MDC9 (ADAM9) have no evident major abnormalities during development or adult life. *Mol. Cell. Biol.* 22: 1537–1544.
19. Horiuchi, K., T. Kimura, T. Miyamoto, H. Takaishi, Y. Okada, Y. Toyama, and C. P. Blobel. 2007. Cutting edge: TNF-α-converting enzyme (TACE/ADAM17) inactivation in mouse myeloid cells prevents lethality from endotoxin shock. *J. Immunol.* 179: 2686–2689.
20. Sahin, U., G. Weskamp, Y. Zheng, V. Chesneau, K. Horiuchi, and C. P. Blobel. 2006. A sensitive method to monitor ectodomain shedding of ligands of the epidermal growth factor receptor. *Methods Mol. Biol.* 327: 99–113.
21. Weskamp, G., J. Schlöndorff, L. Lum, J. D. Becherer, T. W. Kim, P. Saftig, D. Hartmann, G. Murphy, and C. P. Blobel. 2004. Evidence for a critical role of the tumor necrosis factor α convertase (TACE) in ectodomain shedding of the p75 neurotrophin receptor (p75NTR). *J. Biol. Chem.* 279: 4241–4249.
22. Kanazawa, K., and A. Kudo. 2005. Self-assembled RANK induces osteoclastogenesis ligand-independently. *J. Bone Miner. Res.* 20: 2053–2060.
23. Horiuchi, K., S. Le Gall, M. Schulte, T. Yamaguchi, K. Reiss, G. Murphy, Y. Toyama, D. Hartmann, P. Saftig, and C. P. Blobel. 2007. Substrate selectivity of epidermal growth factor-receptor ligand sheddases and their regulation by phorbol esters and calcium influx. *Mol. Biol. Cell* 18: 176–188.
24. Swendeman, S., K. Mendelson, G. Weskamp, K. Horiuchi, U. Deutsch, P. Scherle, A. Hooper, S. Rafii, and C. P. Blobel. 2008. VEGF-A stimulates ADAM17-dependent shedding of VEGFR2 and crosstalk between VEGFR2 and ERK signaling. *Circ. Res.* 103: 916–918.
25. Ye, H., J. R. Arron, B. Lamothe, M. Cirilli, T. Kobayashi, N. K. Shevde, D. Segal, O. K. Dzivenu, M. Vologodskaia, M. Yim, et al. 2002. Distinct molecular mechanism for initiating TRAF6 signalling. *Nature* 418: 443–447.
26. Azuma, Y., K. Kaji, R. Katogi, S. Takeshita, and A. Kudo. 2000. Tumor necrosis factor-α induces differentiation of and bone resorption by osteoclasts. *J. Biol. Chem.* 275: 4858–4864.
27. Murakami, D., I. Okamoto, O. Nagano, Y. Kawano, T. Tomita, T. Iwatsubo, B. De Strooper, E. Yumoto, and H. Saya. 2003. Presenilin-dependent γ-secretase activity mediates the intramembranous cleavage of CD44. *Oncogene* 22: 1511–1516.
28. Nagano, O., and H. Saya. 2004. Mechanism and biological significance of CD44 cleavage. *Cancer Sci.* 95: 930–935.
29. Mumm, J. S., E. H. Schroeter, M. T. Saxena, A. Griesemer, X. Tian, D. J. Pan, W. J. Ray, and R. Kopan. 2000. A ligand-induced extracellular cleavage regulates γ-secretase-like proteolytic activation of Notch1. *Mol. Cell* 5: 197–206.
30. Pinckard, J. K., K. C. Sheehan, C. D. Arthur, and R. D. Schreiber. 1997. Constitutive shedding of both p55 and p75 murine TNF receptors in vivo. *J. Immunol.* 158: 3869–3873.
31. McDermott, M. F., I. Aksentijevich, J. Galon, E. M. McDermott, B. W. Ogunkolade, M. Centola, E. Mansfield, M. Gadina, L. Karenko, T. Pettersson, et al. 1999. Germline mutations in the extracellular domains of the 55 kDa TNF receptor, TNFR1, define a family of dominantly inherited autoinflammatory syndromes. *Cell* 97: 133–144.
32. Xanthoulea, S., M. Pasparakis, S. Kousteni, C. Brakebusch, D. Wallach, J. Bauer, H. Lassmann, and G. Kollias. 2004. Tumor necrosis factor (TNF) receptor shedding controls thresholds of innate immune activation that balance opposing TNF functions in infectious and inflammatory diseases. *J. Exp. Med.* 200: 367–376.
33. Nakagawa, N., M. Kinosaki, K. Yamaguchi, N. Shima, H. Yasuda, K. Yano, T. Morinaga, and K. Higashio. 1998. RANK is the essential signaling receptor for osteoclast differentiation factor in osteoclastogenesis. *Biochem. Biophys. Res. Commun.* 253: 395–400.
34. Oyajobi, B. O., D. M. Anderson, K. Traianedes, P. J. Williams, T. Yoneda, and G. R. Mundy. 2001. Therapeutic efficacy of a soluble receptor activator of nuclear factor kappaB-IgG Fc fusion protein in suppressing bone resorption and hypercalcemia in a model of humoral hypercalcemia of malignancy. *Cancer Res.* 61: 2572–2578.
35. Sordillo, E. M., and R. N. Pearse. 2003. RANK-Fc: a therapeutic antagonist for RANK-L in myeloma. *Cancer* 97(3, Suppl.)802–812.
36. Zhang, J., J. Dai, Z. Yao, Y. Lu, W. Dougall, and E. T. Keller. 2003. Soluble receptor activator of nuclear factor kappaB Fc diminishes prostate cancer progression in bone. *Cancer Res.* 63: 7883–7890.
37. Shipman, C. M., and P. I. Croucher. 2003. Osteoprotegerin is a soluble decoy receptor for tumor necrosis factor-related apoptosis-inducing ligand/Apo2 ligand and can function as a paracrine survival factor for human myeloma cells. *Cancer Res.* 63: 912–916.

Inhibition of STAT1 Accelerates Bone Fracture Healing

Kosuke Tajima,[1] Hironari Takaishi,[1] Jiro Takito,[1] Takahide Tohmonda,[1] Masaki Yoda,[1] Norikazu Ota,[1] Naoto Kosaki,[1] Morio Matsumoto,[1] Hiroyasu Ikegami,[1] Toshiyasu Nakamura,[1] Tokuhiro Kimura,[2] Yasunori Okada,[2] Keisuke Horiuchi,[1] Kazuhiro Chiba,[1] Yoshiaki Toyama[1]

[1]Department of Orthopaedic Surgery, School of Medicine, Keio University, 35 Shinanomachi, Shinjuku, Tokyo 160-8582, Japan, [2]Department of Pathology, School of Medicine, Keio University, 35 Shinanomachi, Shinjuku, Tokyo 160-8582, Japan

Received 12 September 2009; accepted 16 November 2009
Published online 8 January 2010 in Wiley InterScience (www.interscience.wiley.com). DOI 10.1002/jor.21086

ABSTRACT: Skeletal fracture healing involves a variety of cellular and molecular events; however, the mechanisms behind these processes are not fully understood. In the current study, we investigated the potential involvement of the signal transducer and activator of transcription 1 (STAT1), a critical regulator for both osteoclastogenesis and osteoblast differentiation, in skeletal fracture healing. We used a fracture model and a cortical defect model in mice, and found that fracture callus remodeling and membranous ossification are highly accelerated in STAT1-deficient mice. Additionally, we found that STAT1 suppresses Osterix transcript levels and Osterix promoter activity in vitro, indicating the suppression of Osterix transcription as one of the mechanisms behind the inhibitory effect of STAT1 on osteoblast differentiation. Furthermore, we found that fludarabine, a potent STAT1 inhibitor, significantly increases bone formation in a heterotopic ossification model. These results reveal previously unknown functions of STAT1 in skeletal homeostasis and may have important clinical implications for the treatment of skeletal bone fracture. © 2010 Orthopaedic Research Society. Published by Wiley Periodicals, Inc. J Orthop Res 28:937–941, 2010

Keywords: skeletal fracture healing; STAT1; Osterix; fludarabine; NF-κB p65

More than 2 million people each year in the United States suffer from osteoporosis-related fracture, and the financial costs for the patients amounted to as much as $17 billion in 2005,[1] giving a strong incentive to improve the treatment of patients with osteoporotic bone fracture and learn more about bone physiology. Bone healing process involves a variety of molecular and cellular events, which recapitulate, to a certain degree, some of the characteristics of skeletal development;[2,3] however, to date, the molecular mechanisms behind the fracture healing processes are not fully understood.

The signal transducer and activator of transcription 1 (STAT1) was originally identified as a signaling molecule involved in the interferon (IFN) pathway.[4] Interestingly, recent studies revealed that STAT1 participates not only in immune regulations but also in osteoclastogenesis and osteoblast differentiation. It has been shown that both type I and type II interferons (IFN-α/β and IFN-γ) suppress osteoclastogenesis and that STAT1 has critical roles in this IFN-mediated inhibition of osteoclastogenesis.[5] In accordance, *Stat1*$^{-/-}$ mice exhibited an increased osteoclast number and enhanced bone resorption, further corroborating IFN-STAT1 signaling as a critical suppressor of osteoclastogenesis.[6] However, in contrast to these observations, *Stat1*$^{-/-}$ mice showed increased, not decreased, net bone mass with significantly upregulated bone formation, indicating that STAT1 also functions as a potent inhibitor of bone formation in vivo.[7] As expected, the further study revealed that STAT1 suppresses bone formation by directly interacting with Runx2, an essential transcription factor for osteoblast differentiation.[7] These studies have established STAT1 as a critical negative regulator in both bone resorption and bone formation, and, therefore, STAT1 is regarded as a crucial component in the maintenance of skeletal homeostasis in vivo. On the other hand, little is currently known about potential involvements of STAT1 in the bone fracture healing process.

In the current study, we examined the contribution of STAT1 in fracture healing, and found that calcified callus resorption and the subsequent remodeling, as well as membranous ossification were highly accelerated in *Stat1*$^{-/-}$ mice and that STAT1 inhibits the transcription of Osterix (Osx), another essential transcription factor for osteoblast differentiation besides Runx2. Furthermore, we found that fludarabine, a potent STAT1 inhibitor, significantly increases bone formation in a heterotopic ossification model. These results reveal previously unknown contributions of STAT1 in bone fracture healing and may have important clinical implications for the treatment of skeletal bone fracture.

MATERIALS AND METHODS

Animals

Stat1$^{-/-}$ mice[4] were purchased from Taconic Farm Inc. (Hudson, NY, USA). All comparisons described in this study were between the littermates from the crossing between *Stat*$^{+/-}$ mice. The mice were housed in a specific-pathogen free environment and fed with sterile water and feed. All experiments were performed according to the protocol approved by the Laboratory Animal Care and Use Committee of School of Medicine, Keio University.

Bone Fracture Model and Cortical Bone Defect Model

The bone fracture model was performed essentially as previously described with some modifications.[8] In short, under general anesthesia, a transverse osteotomy was performed at the middle of the tibia of 8-week-old male mice with an electric bone saw, and an inner pin of a spinal needle was inserted intramedullary to stabilize the osteotomized bones. A cortical bone defect model in the tibia was performed as previously described.[9] Briefly, under general anesthesia, a round cortical

Correspondence to: Kazuhiro Chiba (T: 81-3-5363-3812; F: 81-3-3353-6597; E-mail: kchiba@sc.itc.keio.ac.jp)

defect 1 mm in diameter was made using a dental burr in the anteromedial aspect of the tibia. The tibiae were collected at the designated time points and were histologically and radiologically evaluated. X-rays and CT images (obtained with Scan Xmate-A090S Comscantecno; Yokohama, Japan) were analyzed by ImageJ software (National Institute of Health) and TRY/3D Bon (Ratoc System Engineering, Tokyo, Japan), respectively.

Cell Culture

COS-7 cells were maintained in Dulbecco's modified Eagle's medium (DMEM; Sigma-Aldrich, St. Louis, MO, USA) containing 10% fetal bovine serum (FBS) and antibiotics. Primary osteoblasts derived from the calvaria (POBs) of newborn mice were prepared as previously described.[1011] POBs and MC3T3-E1 cells were maintained in αMEM (Sigma-Aldrich) containing 10% FBS and antibiotics. To induce osteoblast differentiation, POBs were incubated with αMEM medium supplemented with recombinant human BMP-2 (200 ng/mL, provided by Astellas, Tokyo, Japan), ascorbic acid (50 μg/mL) and β-glycerophosphate disodium salt hydrate (10 mM).

Real-Time RT-PCR

Expression levels for the transcripts for β-actin, Runx2, Osx, and osteocalcin were quantified by RT-PCR using LightCycler (Roche, Basel, Switzerland). cDNA was reverse-transcribed from total RNA prepared from POBs or MC3T3-E1 cells and was used as a PCR template. β-Actin was used as an internal control.

Luciferase Assay

Luciferase reporter vectors bearing *Osx* promoter sequence (−1269/+91) and NF-κB-responsive element (RE) were generously provided by Dr. Mark S. Nanes (Emory University) and Dr. Akihiko Yoshimura (Keio University), respectively. Luciferase reporter vectors were cotransfected with STAT1 or p65 expression vector into MC3T3-E1 or COS-7 cells using Lipofectamine 2000 (Invitrogen, San Diego, CA, USA). Cells were incubated for 48 h and the luciferase activities were measured by Dual-luciferase Reporter Assay Systems (Promega, Madison, WI, USA) as instructed by the manufacturer.

Heterotopic Ossification Model

Recombinant BMP-2 (3 μg) and/or fludarabine (10 μg, Toronto Research Chemicals Inc, Tronto, ON, Canada) was diluted in 10 μL phosphate-buffered saline (PBS) and immersed in gelatin pellets (Gelfoam; Pfizer Inc, New London, CT, USA). The pellets were freeze dried and stored at −20°C until use. The pellets were subcutaneously transplanted in the back of wild-type mice, and were collected 2 weeks after surgery.

Statistical Analysis

Data are presented as mean ± SD. Student's *t*-test for two samples assuming equal variances was used to calculate the *p* values. Values of *p* smaller than 0.05 were considered statistically signficiant. Each experiment was repeated at least three times with similar results.

RESULTS

Stat1$^{-/-}$ Mice Exhibit Accelerated Bone Remodeling in a Murine Fracture Model

To investigate potential involvements of STAT1 in skeletal fracture healing, we utilized a murine bone fracture model as described in Materials and Methods. X-rays and micro CT scanning were performed at 1, 2, 3, 4, 6, and 10 weeks after surgery (Fig. 1A). In wild-type

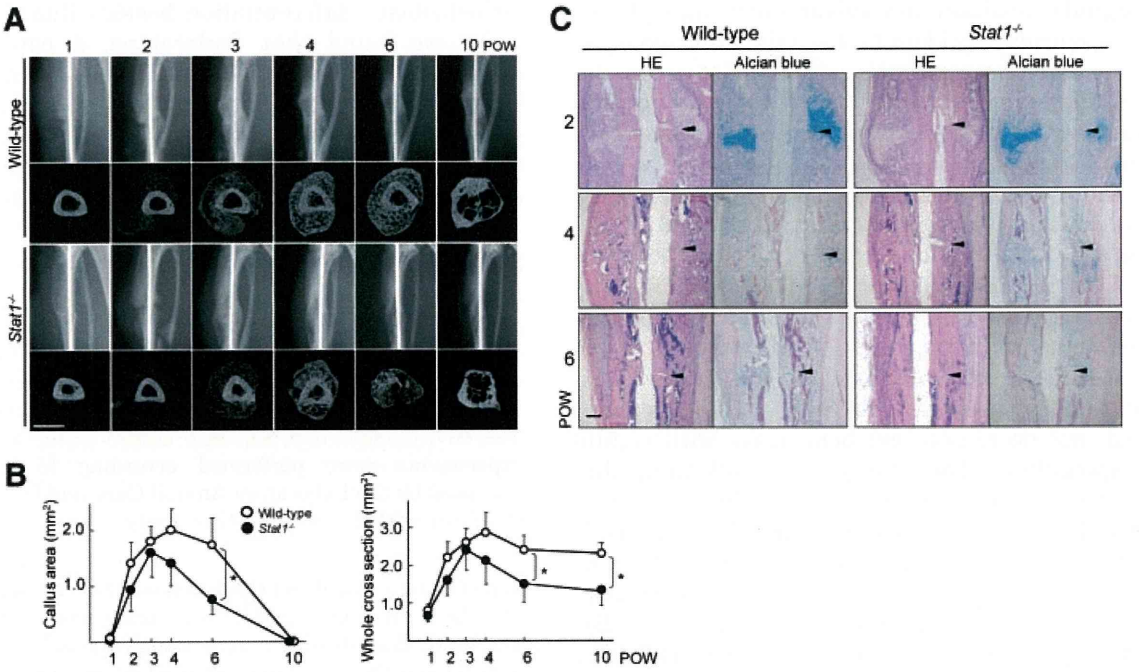

Figure 1. *Stat1*$^{-/-}$ mice exhibit accelerated bone healing. (A) X-ray images (upper row) and micro-CT images (lower row) of the fractured tibiae in wild-type and *Stat1*$^{-/-}$ mice. Scale bar, 1 mm. (B) Sequential changes of the cross-sectional callus area of the fracture site (left panel) and of the whole cross-sectional area of tibia (which includes the tibia itself and the fracture callus; right panel) at the fracture-site analyzed on axial CT images. $n = 4$. *$p < 0.05$. (C) Sections of osteotomized tibia from wild-type and *Stat1*$^{-/-}$ mice stained with hematoxylin-eosin or alcian blue. Note that there was no apparent difference in the cartilage formation between wild-type and *Stat1*$^{-/-}$ mice; however the remodeling of callus was accelerated in *Stat1*$^{-/-}$ mice. Arrowheads, fractured site. Scale bar, 100 μm.